

AD-A039 797

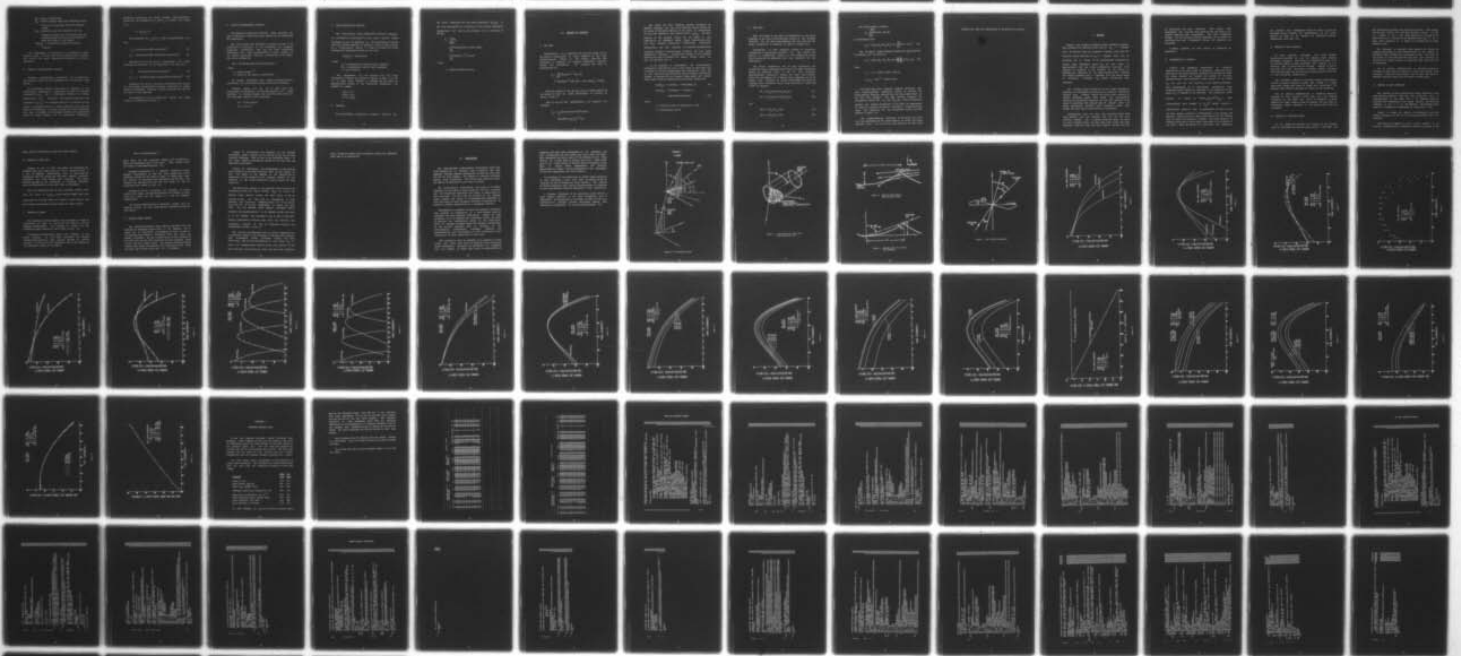
NAVAL POSTGRADUATE SCHOOL MONTEREY CALIF  
POWER-DENSITY DISTRIBUTION BELOW THE OCEAN SURFACE DUE TO INCID--ETC(U)  
MAR 77 M J MILCHANOWSKI

F/G 20/6

UNCLASSIFIED

NL

| OF |  
AD  
A039797



END  
DATE  
FILMED  
6-77

ADA 039797

# NAVAL POSTGRADUATE SCHOOL

Monterey, California



9 Master's **THESIS**

6 POWER-DENSITY DISTRIBUTION BELOW THE OCEAN SURFACE DUE TO INCIDENT LASER RADIATION

by

10 Michael John Milchanowski

11 March 1977

12 85p.

Thesis Advisor: D. J. Collins

Approved for public release; distribution unlimited.

AD No. ———  
DDC FILE COPY

251 450 ♀

DDC  
RECEIVED  
MAY 24 1977  
RECEIVED

A

REPORT DOCUMENTATION PAGE		READ INSTRUCTIONS BEFORE COMPLETING FORM
1. REPORT NUMBER	2. GOVT ACCESSION NO.	3. RECIPIENT'S CATALOG NUMBER
4. TITLE (and Subtitle) POWER-DENSITY DISTRIBUTION BELOW THE OCEAN SURFACE DUE TO INCIDENT LASER RADIATION		5. TYPE OF REPORT & PERIOD COVERED Master's Thesis; (March 1977)
		6. PERFORMING ORG. REPORT NUMBER
7. AUTHOR(s) Michael John Milchanowski		8. CONTRACT OR GRANT NUMBER(s)
9. PERFORMING ORGANIZATION NAME AND ADDRESS Naval Postgraduate School Monterey, California 93940		10. PROGRAM ELEMENT, PROJECT, TASK AREA & WORK UNIT NUMBERS
11. CONTROLLING OFFICE NAME AND ADDRESS Naval Postgraduate School Monterey, California 93940		12. REPORT DATE March 1977
		13. NUMBER OF PAGES 85
14. MONITORING AGENCY NAME & ADDRESS (if different from Controlling Office) Naval Postgraduate School Monterey, California 93940		18. SECURITY CLASS. (of this report) Unclassified
		18a. DECLASSIFICATION/DOWNGRADING SCHEDULE
16. DISTRIBUTION STATEMENT (of this Report) Approved for public release; distribution unlimited.		
17. DISTRIBUTION STATEMENT (of the abstract entered in Block 20, if different from Report)		
18. SUPPLEMENTARY NOTES		
19. KEY WORDS (Continue on reverse side if necessary and identify by block number) Laser, Ocean		
20. ABSTRACT (Continue on reverse side if necessary and identify by block number) The time-averaged power-density distribution below the ocean surface due to incident laser radiation is examined by means of computer simulation of the geometrical optics involved with the air/sea interface and subsequent ocean penetration by the laser beam. The effects over the entire spectra of incidence angles, → next page		

cont

→ wind velocities, wind directions, beam spot sizes and depths of penetration are analyzed.



CLASSIFIED BY	
DTIC	State Section <input checked="" type="checkbox"/>
DDI	Dist Section <input type="checkbox"/>
UNCLASSIFIED	
JUSTIFICATION	
BY	
DISTRIBUTION/AVAILABILITY CODES	
GENL	AVAIL. AND/OR SPECIAL

Approved for public release; distribution unlimited.

POWER-DENSITY DISTRIBUTION BELOW THE OCEAN SURFACE DUE TO  
INCIDENT LASER RADIATION

by

Michael John Milchanowski  
Lieutenant, United States Navy  
B.S., United States Naval Academy, 1969  
M.S., University of West Florida, 1971

Submitted in partial fulfillment of the  
requirements for the degree of

MASTER OF SCIENCE IN AERONAUTICAL ENGINEERING

from the  
NAVAL POSTGRADUATE SCHOOL  
March 1977

Author:

*Michael John Milchanowski*

Approved by:

*Daniel L. Collins*

Thesis Advisor

*Therese H. Gausman*

Second Reader

*Richard W. Bell*

Chairman, Department of Aeronautics

*Robert A. Johnson*

Dean of Science and Engineering

## ABSTRACT

The time-averaged power-density distribution below the ocean surface due to incident laser radiation is examined by means of computer simulation of the geometrical optics involved with the air/sea interface and subsequent ocean penetration by the laser beam. The effects over the entire spectra of incidence angles, wind velocities, wind directions, beam spot sizes and depths of penetration are analyzed.

## TABLE OF CONTENTS

I.	INTRODUCTION.....	6
II.	DESCRIPTION OF PHYSICAL PARAMETERS.....	7
	A. OCEAN SURFACE.....	7
	B. LASER BEAM.....	8
	C. MAXIMUM ANGLE OF INCIDENCE.....	9
III.	POWER-DENSITY PROBABILITY INTEGRAL.....	11
	A. GENERAL EQUATION.....	11
	B. FRESNEL'S TRANSMITTANCE FUNCTION.....	12
	C. DIFFUSE TRANSMITTANCE FUNCTION.....	14
	D. SLOPE PROBABILITY FUNCTION.....	15
	E. JACOBIAN.....	15
IV.	METHODS OF SOLUTION.....	17
	A. FAR ZONE.....	17
	B. NEAR ZONE.....	19
V.	RESULTS.....	22
	A. PRESENTATION OF RESULTS.....	23
	B. EFFECTS OF WIND VELOCITY.....	24
	C. EFFECTS OF INCIDENCE ANGLE.....	24
	D. EFFECTS OF WIND DIRECTION.....	25
	E. EFFECTS OF SPOT SIZE.....	26
	F. EFFECTS OF DEPTH.....	26
	G. MAXIMUM POWER DENSITY.....	27
VI.	CONCLUSIONS.....	30
	Appendix A: FIGURES.....	32
	Appendix B: COMPUTER PROGRAM USAGE.....	56
	NEAR ZONE COMPUTER PROGRAM.....	60
	FAR ZONE COMPUTER PROGRAM.....	67
	COMMON COMPUTER SUBROUTINES.....	71
	LIST OF REFERENCES.....	82
	INITIAL DISTRIBUTION LIST.....	85

## I. INTRODUCTION

The time-averaged power-density distribution below the ocean surface due to incident laser radiation is examined over the entire spectra of incidence angles, wind velocities and wind directions by means of geometrical optics.

Current interest in using laser systems for communications through the air-sea interface and for detecting submerged objects necessitates the development of prediction methods for determining the subsurface power-distribution of radiation from a laser source above the ocean. A mathematical model for the optical-communications application done by Karp in Ref. 1 is developed in terms of a radiance function related to the mutual coherence function with accurate results for incidence angles out to 45 degrees. A more general model developed by Swennen in Refs. 2-4 examines the power-density distribution below the ocean surface through a rigorous assessment of the ocean surface geometry allowing for theoretically accurate results over the entire incidence angle spectrum.

The computer code developed for this analysis of the power-density distribution below the ocean surface is an expansion of Swennen's theory[Refs. 2-4].

## II. DESCRIPTION OF PHYSICAL PARAMETERS

### A. OCEAN SURFACE

A geometrical representation of the ocean surface in terms of local slopes developed by Cox and Munk[Ref. 5] is the basis for the analysis of the power probability distribution below the ocean, as it is in Refs. 2-4. A review of this representation follows.

The center of symmetry of the incident laser beam on the ocean surface facet is the center of a right-handed cartesian coordinate system, point "0" in Fig. 1. The z-axis points vertically upward. The y-axis is in the horizontal plane, colinear with the projection of the center of the incident laser beam onto that plane and pointing in the direction of the laser source.

The slopes of the ocean surface facet are defined by angular parameters Alpha and Beta. The angle Beta is the angle between the line of steepest ascent of the facet and the x-y plane; Alpha is the angle between the projection of the line of steepest ascent onto the x-y plane and the y-axis.

A second cartesian coordinate system at the surface is used, as explained in Ref. 2, to simplify the computation of the slope probability function. This coordinate system is designated by primes with the y'-axis pointing towards the wind source and rotated an angle Chi from the y-axis. The

$z'$ -axis coincides with the  $z$ -axis. The slope parameters are also primed with their transformations given by:

$$\text{Beta}' = \text{Beta}$$

$$\text{Alpha}' = \text{Alpha} - \text{Chi}$$

Below the ocean surface a depth  $Z$  at the point of observation,  $O'$ , is centered a translational transformation of the surface coordinate system. Angles  $\mu$  and  $\nu$  define the laser beam refracted to  $O'$  by any surface facet. The first angle,  $\mu$ , is the angle between the refracted ray and the  $z$ -axis; the second,  $\nu$ , is the angle between the  $y$ -axis and the vertical plane of the refracted ray.

#### B. LASER BEAM

A cylindrical laser beam of radius  $a$  is incident on the ocean surface wave facet at an angle  $\psi$  measured from the  $z$ -axis. The intersection of the beam and the facet is a flat elliptical surface as illustrated in Fig. 2. The semi-minor axis of the ellipse is equal to the beam radius and the semi-major axis,  $b$ , is defined by:

$$b = a * \sec \psi$$

The analytical development, as in Refs. 2-4, begins at the ocean surface facet. The laser source, aiming, atmospheric propagation, etc. are extraneous to this analysis. Power density values at the surface are not quoted because the analysis deals with the ratio of the

power density at the depth of interest,  $P_d$ , and the power density at the surface,  $P_{ds}$ .

### C. MAXIMUM ANGLE OF INCIDENCE

The angle of incidence with respect to the z-axis,  $\Psi$ , of the laser beam is analyzed from zero degrees to a maximum of 84 degrees. At greater angles the beam will not be able to strike all the wave facets within a wavelength of the wave due to the wave height. There is also the possibility, as illustrated in Fig. 3, that a ray incident at  $\Psi > 84$  degrees could pass through the wave, re-enter the atmosphere and then re-enter the ocean; or, depending on the local slopes, the ray could undergo a total internal reflection if the Critical Angle were exceeded. The mathematical model of Swennen[Refs. 2-4] and this thesis do not address this situation.

This limitation on the maximum angle of incidence,  $\Psi_{max}$ , is derived from Fig. 4 and defined by:

$$\Psi_{max} = \tan^{-1}(L/2H)$$

The significant wave height,  $H$ , and the average period,  $T$ , of the wave are given by equations (1) and (2) as defined by Pierson[Ref. 7]. The average wavelength of the wave is given by equation (3) as defined by Hill[Ref. 8].

$$H = 2.14 \times 10^{-2} * W^2 \quad (1)$$

$$T = 0.81 * (2W/g) \quad (2)$$

$$L = gT^2 / 2 \quad (3)$$

where

W = wind velocity

g = gravitational constant

For wind velocities of 1 to 14 m/sec the maximum angle of incidence is 84.2 degrees ( $\pm 0.4$  degrees) for all wind velocities; therefore,  $\Psi_{\max}$  is limited to 84 degrees.

### III. POWER-DENSITY PROBABILITY INTEGRAL

#### A. GENERAL EQUATION

The power-density probability distribution ( $P_d$ ) at the point of observation below the ocean surface ( $O'$ ) due to the entire beam is given by the integral of  $dP_d$  over all of the contributing surface facets. As a function of the angular parameters ( $\mu, \nu$ ) the integral as defined in Refs. 2-4 is given by:

$$P_d = \iint_{\mu \nu} F(\mu, \nu) d\mu d\nu \quad (4)$$

where

$$F(\mu, \nu) = P_{ds} * T * DTF * \cos(WI) * \sec(WR)$$

$$* [ \cos(\mu) * \cos(\mu_0) + \sin(\mu) * \sin(\mu_0) * \cos|\nu - \nu_0| ]$$

$$* P_{xy}(z', z') * \tan(\beta) * \sec^2(\beta) * J^{-1}$$

and

$P_{ds}$  = power density at the surface facet

$T$  = Fresnel's transmittance coefficient

$DTF$  = diffuse transmittance function

$WI$  = angle of incidence

WR = angle of refraction

$\mu_0$  = first quadrant angle the refracted center ray of the beam makes with the positive z-axis

$\nu_0$  = positive angle the projection of the refracted center ray of the beam onto the xy-plane makes with the y-axis measured from the latter to the former

$F(Z'_x, Z'_y)$  = time-average slope distribution function

The development of equation (4) is described in great detail in Refs. 2-4 and will not be repeated here; however, for clarity the major components of equation (4) will be discussed.

#### B. FRESNEL'S TRANSMITTANCE FUNCTION

Fresnel's transmittance coefficient (T) is defined as the intensity ratio of the transmitted to the incident beam energy.

The collimated incident laser beam is composed of two polarization components, a transverse magnetic or parallel polarization ( $T_{//}$ ) and a transverse electric or normal polarization ( $T_{\perp}$ ). Resolving the refracted beam into its components ( $T_{\perp}, T_{//}$ ) is a complex task due to rotation of the plane of incidence about all three coordinate axis over the range of integration. In order to deal with this complexity the beam is assumed to be rendered diffuse and unpolarized below the ocean surface due to scattering, propagation

direction variations and phase changes. This assumption allows for the averaging of  $T_{\perp}$  and  $T_{\parallel}$  to obtain the value of  $T$ .

$$T = (T_{\perp} + T_{\parallel}) / 2$$

The equations for  $T_{\perp}$  and  $T_{\parallel}$  used by Swennen [Refs. 2-4] are:

$$T_{\perp} = [\sin(WI) * \sin(WR) / \sin(WI+WR)]^2 \quad (5)$$

$$T_{\parallel} = [\sin(WI) * \sin(WR) / \sin(WI+WR) * \cos(WI-WR)]^2 \quad (6)$$

Equations (5) and (6) are in disagreement with those developed by Born [Ref. 9] and Fowles [Ref. 10], given by:

$$T_{\perp} = [2 * \cos(WI) * \sin(WR) / \sin(WI+WR)]^2 \quad (7)$$

$$T_{\parallel} = [\cos(WI) * \sin(WR) // \sin(WI+WR) * \cos(WI-WR)]^2 \quad (8)$$

Equations (5) and (6) will give erroneously high values for the Fresnel transmittance function, especially at higher angles of incidence. Because of this, equations (7) and (8) are used in this modeling.

The geometry of the ray refraction through the ocean surface is illustrated in Fig. 5.

### C. DIFFUSE TRANSMITTANCE FUNCTION

The diffuse transmittance function (DTF) accounts for beam attenuation below the ocean surface due to scattering and absorption.

The six-constant DTF developed by Duntley in Ref. 11 is simplified to a function of two constants; the backward scattering coefficient (BS) and the total absorption coefficient (AC). This simplification is valid because of the random scattering particle orientation in the ocean. The DTF is defined by:

$$DTF = K / [ (AC+BS) * \sinh(K*Z) + K * \cosh(K*Z) ]$$

where

$$K = [ AC * (AC + 2BS) ]^{1/2}$$

Z = depth of the point of observation

In current terminology this method of accounting for attenuation is a zero-angle forward scattering technique.

Typical values for BS and AC were used from measurements by Tyler [Ref. 12] and Duntley [Ref. 13]. These represent an average between cool and warm ocean waters in the blue-green spectrum (4800 angstrom).

$$BS = 0.065 \text{ percent}$$

$$AC = 0.044 \text{ m}^{-1}$$

#### D. SLOPE PROBABILITY FUNCTION

The time-average slope probability function,  $P(Z'_x, Z'_y)$ , is a statistical distribution of the ocean surface slopes developed by Cox and Munk[Ref. 5]. The distribution derived from the surface geometry is Gaussian, which is then altered by a Gram-Charlier series in order to account for slope skewness and peakedness caused by the wind.

$$P(Z'_x, Z'_y) = f(X_i, \text{Eta}, W)$$

where

$X_i$  = standardized crosswind slope component

$\text{Eta}$  = standardized upwind slope component

$W$  = wind velocity

The development and the equation for the slope probability function are covered in detail in Refs. 2, 4, and 5. A clean ocean surface is assumed and the limits of applicability placed on the functional parameters are adhered to, namely:

$$|X_i| \leq 2.5$$

$$|\text{Eta}| \leq 2.5$$

$$W \leq 14 \text{ m/sec}$$

#### E. JACOBIAN

The power-density probability integral, equation (4),

was first developed over the slope components  $(Z'_x, Z'_y)$ . It was then transformed to a function of the angular parameters  $(\text{Alpha}, \text{Beta})$  and then by the Jacobian  $(J)$  to a function of  $(\text{Mu}, \text{Nu})$ .

$$\begin{aligned}
 P_d &= \iint_{Z'_x, Z'_y} dP_d \\
 &= \iint_{\alpha \beta} F(\text{Alpha}, \text{Beta}) d\text{Alpha} d\text{Beta} \\
 &= \iint_{\mu \nu} F(\text{Mu}, \text{Nu}) J^{-1} d\text{Mu} d\text{Nu}
 \end{aligned}$$

where

$$J = \partial(\text{Mu}, \text{Nu}) / \partial(\text{Alpha}, \text{Beta})$$

#### IV. METHODS OF SOLUTION

##### A. FAR ZONE

Swennen[Refs. 2-4] observed that when the depth (Z) of the point of observation is large compared to the beam cross-sectional radius at the surface (Z/a>100) the integrand of equation (4) remains essentially constant during the integration. The integral can then be approximated by:

$$P_d = \iint_{\mu\nu} F(\mu, \nu) * J^{-1} d\mu d\nu$$

$$\approx F(\mu, \nu) * J^{-1} \Delta\mu \Delta\nu ; \text{ with } \mu = \mu_0 \text{ \& } \nu = \nu_0$$

The area  $\Delta\mu\Delta\nu$  in the  $(\mu, \nu)$  plane is approximated by an ellipse of area  $\Delta A$ , whose development is covered in detail in Ref. 3.

This is the Far Zone approximation and equation (4) becomes:

$$P_d = P_{ds} * T * \tan(\beta) * \sec^2 * \cos(WI)$$

$$* \sec(WR) * P \left( \begin{matrix} Z' \\ x \end{matrix}, \begin{matrix} P' \\ y \end{matrix} \right) * J^{-1} * \Delta A$$

The basic Far Zone computer program developed in FORTRAN language and run on the IBM 360 system solves for the ratio of the power density at the point of observation to the power density at the surface facet,  $P_d/P_{ds}$ . The main portion of the program allows for the entry of any combination of variables (wind, depth, beam radius, Psi, Chi,  $Nu_0$ , backward scattering coefficient, absorption coefficient), and also computes the diffuse transmittance function, Fresnel's transmittance function and the slope probability function. Subroutines common to all variable entries are used to compute the angles (Alpha, Beta, WI, WR), the Jacobian and A.

It is possible to investigate the power-density probability distribution over a wide range of variables with a minimal of storage requirements and computation time due to the use of an IBM System/360 Source Library subroutine, NLNSYS, in solving for the coupled (Alpha, Beta) and (Mu, Nu) angle pairs from the simultaneous non-linear equations:

$$\cos(\mu_0) = [\cos(\Psi) + K \cdot \cos(\beta)]/n \quad (9)$$

$$\cot(\nu_0) = \cot(\alpha) - \sin(\Psi)/K \\ * \sin(\alpha) * \sin(\beta) \quad (10)$$

where

$n$  = relative index of refraction (1.33)

$K = K(\Psi, \alpha, \beta, n)$

## B. NEAR ZONE

When the depth of the point of observation is not large compared to the beam cross-sectional radius at the surface ( $Z/a < 100$ ) the Far Zone approximation does not hold and the double integration of equation (4) must be carried out.

Swennen[Ref. 2] used Simpson's method of numerical integration to approximate equation (4). The method was subject to singularity points in the integration limits which increased the complexity and time required for the computation.

The double integration can be more accurately and relatively simply approximated by using the Gauss Quadrature system of solution, Refs. 14 and 15. The Two-Point Gauss-Legendre Quadrature method was used. This method, valid for polynomials up to degree three (equation (4) is of degree two), consists of first transforming the function  $F(\mu, \nu)$  into a function  $F(s, t)$  whose interval is  $-1 \leq s \leq 1$  and  $-1 \leq t \leq 1$  by letting:

$$\mu = [(\mu_u - \mu_l) * s + \mu_u + \mu_l] / 2 \quad (11)$$

$$\nu = [(\nu_u - \nu_l) * t + \nu_u + \nu_l] / 2 \quad (12)$$

and

$$d\mu = [(\mu_u - \mu_l) / 2] ds \quad (13)$$

$$d\nu = [(\nu_u - \nu_l) / 2] dt \quad (14)$$

The power-density integral

$$P_d = \int_{\mu_1}^{\mu_u} \int_{\nu_1}^{\nu_u} F(\mu, \nu) d\mu d\nu$$

is transformed into

$$P_d = [(\mu_u - \mu_1)(\nu_u - \nu_1)/4] * \int_{-1}^1 \int_{-1}^1 F(s, t) ds dt \quad (15)$$

The Two-Point Gauss-Legendre Quadrature approximation of equation (13) is given by:

$$P_d = [(\mu_u - \mu_1)(\nu_u - \nu_1)/4] * \sum_{i=0}^1 \sum_{j=0}^1 W_i * P(s_i, t_j) \quad (16)$$

where

$$W_i = 1.0 = \text{Gauss weight factors}$$

$$s_i, t_j = \pm(3)^{-2} = \text{Gauss roots}$$

The basic Near Zone computer program developed uses this Gauss-Legendre Quadrature method in solving the power-density integral coupled with the same subroutines as the Far Zone program. The main program computes the integration limits  $(\mu_u, \mu_1)$  and  $(\nu_u, \nu_1)$  after determining whether the surface projection of the point of observation is inside or outside the beam's horizontal cross-sectional area. The equations for the integration limits are well defined in Refs. 2-4.

The transformations described by equations (11)-(15) are then performed and the power-density is solved for using equation (16). As in the Far Zone program, the Near Zone

program can take any combination of variables as entries.

## V. RESULTS

Results for oblique incidence angles ( $0 < \Psi \leq 84$  degrees) were obtained for vertical plane cuts at  $Nu_0 = 0$  degrees over the entire range of variables; however, valid data for vertical planar sections at  $Nu_0 \neq 0$  degrees could not be obtained due to values of the standardized crosswind and upwind slope components being out of the range of applicability for the slope probability function. This problem is believed to be inherent in the method of mathematical analysis of the ocean surface used. Results for normal incidence ( $\Psi = 0$  degrees) over the entire range of variables, including  $Nu_0$  planar variations, were obtained.

The validity check carried out on the slope probability function, as discussed in Section III.D, clearly identified invalid data. Another source of invalid data occurred at higher incidence angles ( $\Psi$ ) where the simultaneous solution of non-linear equations (9) and (10) resulted in an angle of incidence ( $WI$ ) greater than 90 degrees while the slope probability function still indicated valid. This output was also easily identified and eliminated.

Computations with the Near Zone solution method used more computer time and storage than did the Far Zone solution method. For a computer solution using one value for each variable entry, the Near Zone used 36 per cent more computer time and 8 per cent more computer storage than did

an equivalent Far Zone solution. The higher time requirement for the Near Zone solution was due mainly to a greater compiling time requirement. The time difference between the two solution methods decreased as the number of variables that were incremented during one computer run increased.

A sample computer run with output is presented in Appendix E.

#### A. PRESENTATION OF RESULTS

Results are presented graphically to simplify comparisons of the wide range of variables. Vertical-planar sections of the power density probability distribution below the ocean surface cut through the center of the beam cross-section at the horizontal ocean surface at an angle  $\mu_0$  are used for the majority of the results presented.

This presentation is in rectangular coordinates with normalized power density in decibels on the ordinate and the angle  $\mu_0$  in degrees on the abscissa. The normalized power

density is equal to  $10 \cdot \log_{10} [(P_d \cdot Z^2) / P_{ds}]$ . This normalization with respect to  $P_{ds} / Z^2$  should produce a

distribution function that is independent of depth in the Far Zone regime, according to Swennen[Ref. 2-4], because the multiple slopes seen in a beam cross-section at the surface tend to render the radiation diffuse. The power density of diffuse radiation at large depths decreases as the square of the depth. When the effects of scattering and absorption

are included this independence does not occur, as will be discussed later; however, the normalization of the power density is used in all regimes for continuity and for comparisons with Refs. 2-4.

#### E. EFFECTS OF WIND VELOCITY

As wind velocity increases, the power density distribution spreads out and the maximum power density decreases slightly. This effect is presented in Figs. 6-11 for various angles of beam incidence with respect to the vertical ( $\Psi = 0, 30, 60$  and  $84$  degrees). Figures 10 and 11 also show the close correlation between results obtained from the Near Zone and the Far Zone solution methods for  $\Psi = 0$  and  $40$  degrees, respectively.

The spreading effect on the power density distribution is due to larger refraction angles (WR) caused by higher wave facet slopes that occur at higher wind velocities. The maximum power density decrease is caused by the spreading.

For an optical communication or detection system an increase in wind velocity would mean that the maximum intensity of the beam that could be focused to a point beneath the ocean surface would be reduced, but the width of receivable signal radiation or the search width would be increased.

#### C. EFFECTS OF INCIDENCE ANGLE

As the angle of incidence with respect to the vertical ( $\Psi$ ) is increased the maximum power density decreases and

the distribution shifts away from the vertical. This effect can be seen in Figs. 6-11 and more clearly in Figs. 12 and 13. Figure 12 is a Far Zone solution at a depth of 50 meters for  $\Psi = 0, 30, 60$  and  $84$  degrees while Fig. 13 is a Near Zone solution at a depth of 10 meters for the same values of  $\Psi$ .

The decrease in maximum power density is a result of greater reflectance at the surface facet as the angles of incidence ( $WI$ ) increase with increases in  $\Psi$ . The shift in the center of the distributions away from the vertical is caused by the higher angles of refraction ( $WR$ ) that occur as  $WI$  increases.

For an optical communication or detection system an increase in  $\Psi$  would be expected to lower the maximum beam intensity below the ocean surface and to shift the point of maximum intensity away from the point of water entry.

#### D. EFFECTS OF WIND DIRECTION

The effects of wind direction are small compared to the wind velocity effects. When the wind direction ( $\chi$ ) is perpendicular to the beam ( $\chi = 90$  degrees) there is slightly less spreading of the power density distribution compared to  $\chi = 0$  or  $180$  degrees. The maximum power density is essentially unaffected by variations in  $\chi$ .

Figure 14 shows the effect of variations in  $\chi$  for normal incidence and Fig. 15 for oblique incidence ( $\Psi = 40$  degrees).

Wind direction appears to be of little concern to an optical communication or detection system as related to the

power density distribution below the ocean surface.

#### E. EFFECTS OF SPOT SIZE

Figures 16 and 17 show the effect of increasing the incident beam spot radius from 0.1 to 0.5 meters for  $\Psi = 0$  and 40 degrees, respectively. This is done with the assumption that the energy per unit area remains constant; therefore, the total energy must increase. The power density spreads out and increases in intensity uniformly over the distribution as the spot size is increased.

Since the equations used in this solution method deal with the ratio of  $P_d/P_{ds}$ , these results simply mean that more power in a larger beam will produce a more intense and more widely distributed pattern below the ocean surface.

#### F. EFFECTS OF DEPTH

The decrease of power density with increases in depth is illustrated in Figs. 18 and 19 for  $\Psi$  equal to 0 and 40 degrees, respectively. The decrease is linear for the normalized power density as can be seen in Fig. 20.

Scattering and absorption cause this decrease in the power density. As the depth increases the diffuse transmittance function (DTF) rapidly becomes an inverse function of the sum of the hyperbolic sine of the depth and the hyperbolic cosine of the depth,

$$DTF = f[ (\sinh Z + \cosh Z)^{-1} ]$$

which means the DTF decreases rapidly with increases in depth and approaches zero in the limit. This agrees with the theory of Preisendorfer [Ref. 16].

Swennen's prediction of a constant normalized power density distribution in the Far Zone regime due to the diffusing effects of the ocean in Refs. 2-4 holds only when the effects of scattering and absorption are ignored. One computer run was made with the DTF set equal to one to illustrate this effect in Fig. 20.

Figures 21 and 22 illustrate the decrease in power density with depth, non-dimensionalized with respect to spot size,  $Z/a$ , again for  $\Psi$  equal to 0 and 40 degrees, respectively.

An optical communication or detection system will be limited greatly by the power density decrease associated with depth.

#### G. MAXIMUM POWER DENSITY

The maximum obtainable power density available over the spectrum of incidence angles ( $\Psi = 0 - 84$  degrees) for a given set of conditions is presented in Figs. 23 and 24. The maximum power density obtainable does not occur for normal incidence, but for a small value of  $\Psi$ , because of the fact that as the wind increases the most probable slope is not zero but a small angle. The maximum obtainable power density then drops continuously with increases in  $\Psi$  after the peak that occurs around  $\Psi = 10 - 15$  degrees.

Figure 23 illustrates the decrease in the maximum obtainable power density for all values of  $\Psi$  as the wind velocity increases. This is due to the spreading effect on the power density distribution caused by the wind that was described previously.

Figure 24 illustrates the independence of the maximum power density on the wind direction ( $\chi$ ) for all values of  $\Psi$ .  $\chi$  equal to 270 degrees is not plotted but is equivalent to the condition at 90 degrees because of the symmetry of the slope probability function about the wind direction.

The angle with respect to the vertical from the point of observation below the ocean surface ( $\mu_0$ ) at which the maximum power density occurs for each value of  $\Psi$  is plotted in Fig. 25. The plot is independent of wind velocity and direction. Examining Figs. 16 - 19 it can be seen that Fig. 25 is also independent of depth and spot size.  $\mu_0$  for maximum power density increases nearly linearly from approximately 1 to 56 degrees as  $\Psi$  goes from 0 to 84 degrees. The increase in  $\mu_0$  is due to the power density distribution shifting away from the vertical for increasing values of  $\Psi$  as discussed earlier and illustrated in Figs. 12 and 13.

The obvious consideration with an optical communication or detection system is the decrease in maximum power density that accompanies higher incidence angles and wind velocities. The strong independence of the angle  $\mu_0$  at which the maximum power density occurs with respect to the wind velocity, wind direction, depth and spot size indicates

that a satellite based laser navigation system for submarine usage may be a possibility.

## VI. CONCLUSIONS

The time-averaged power-density distribution below the ocean surface due to incident laser radiation has been examined through computer simulations in both the Near Zone and the Far Zone regimes. The effects of altering incidence angles, wind velocities, wind directions, beam spot sizes and depths of penetration have been presented.

The power-density distribution was found to be highly dependent on the angle of beam incidence, the wind velocity and the attenuation associated with depth of penetration of the laser beam. The fact that the location of the maximum power density was found to be fundamentally dependent on only the angle of beam incidence indicates a possibility of direction finding capabilities by a submerged receiver.

Improvements in computer systems and analysis techniques have allowed an examination of a much broader range of variables than were possible heretofore. Angles of beam incidence up to 84 degrees were considered within the range of validity for restrictions placed on the simulation. Above 84 degrees incidence angle the possible interactions at the air/sea interface make an analysis of the power-density distribution extremely complex, and experimentation will be necessary to give indications of the feasibility of laser operations in this area.

This simulation could be extended to an analysis of much larger spot sizes that would be expected from a satellite based transmitter. Prettyman and Cermak[Ref. 17] suggested that the effects of larger spots could be approximated by

assuming each wave facet independent of its neighbors and then integrating over the larger spot area, since the small spot represents the outer limit of the effects of the ocean surface on a laser beam of greater spot size. There would have to be a large number of surface facets contained in the spot to insure facet independence and accurate approximations, hence a strong dependence on the wavelength of the wave associated with wind velocity.

An extension of the simulation to pulsed laser radiation is also warranted, since this mode of operation may be required for air-to-subsurface laser systems. The effects of pulsed radiation occur nearly instantaneously as compared to the time-averaged analysis performed in this simulation.

A further refinement of the simulation would involve a more complex modeling of the beam attenuation due to scattering and absorption in the ocean through the use of a diffusion or a multiple forward scattering method, both described by Bucher[Ref. 18] and Preisendorfer[Ref. 16].

APPENDIX A

FIGURES

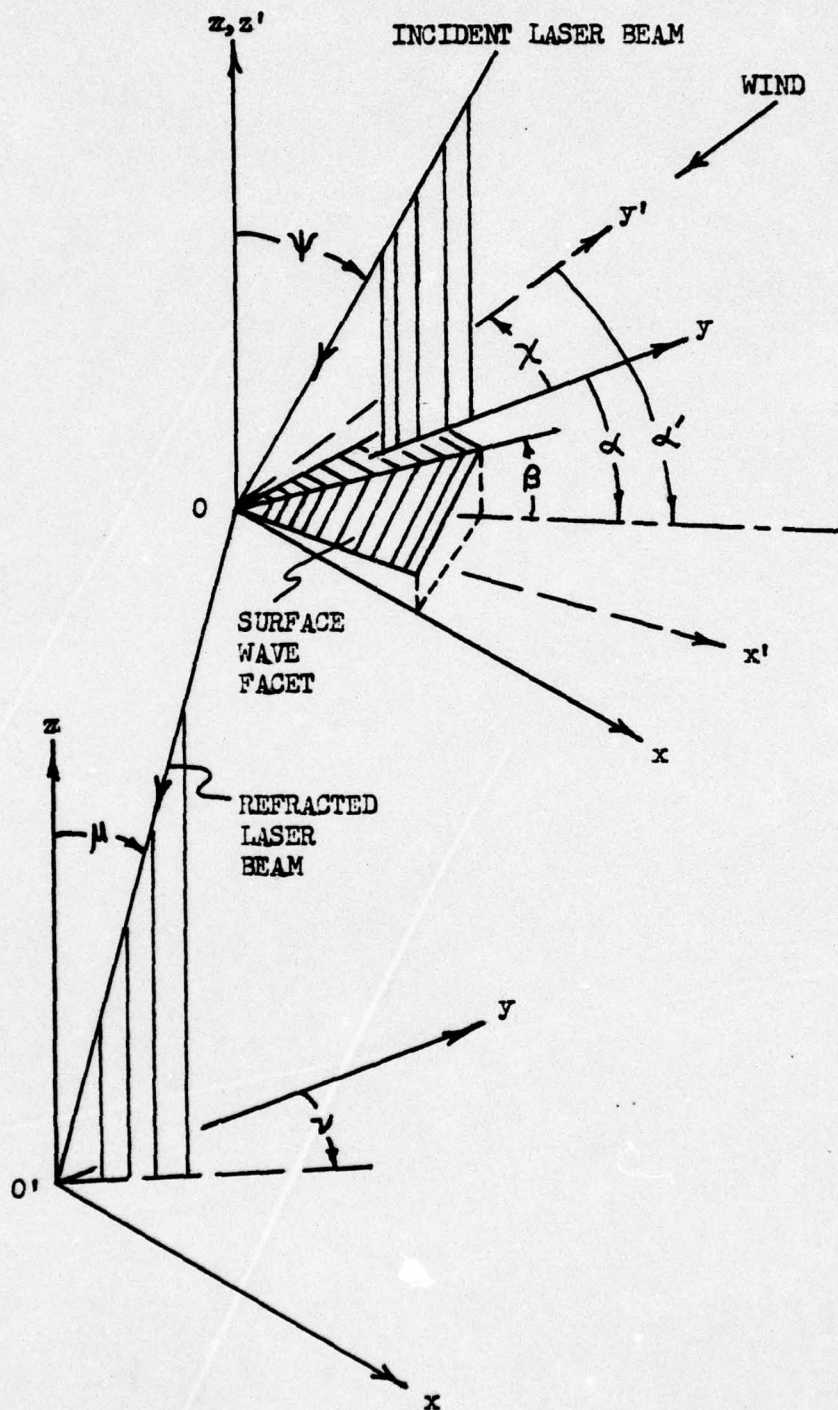


Figure 1: Coordinate systems

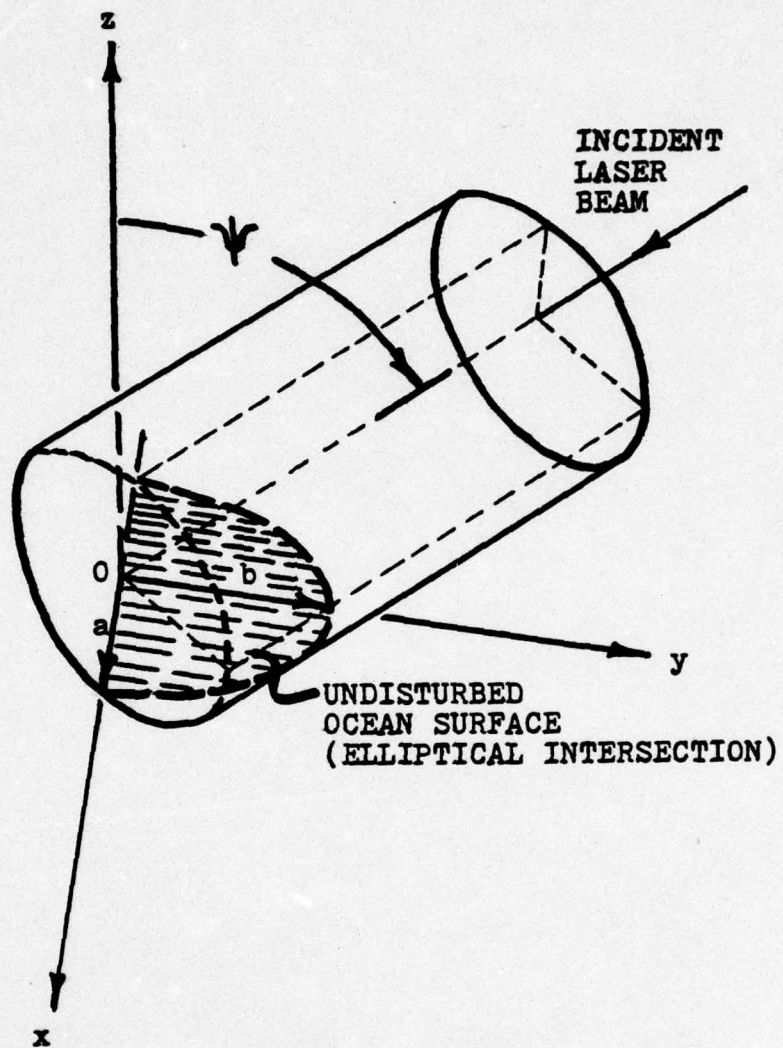


Figure 2: Intersection of laser beam with ocean wave facet

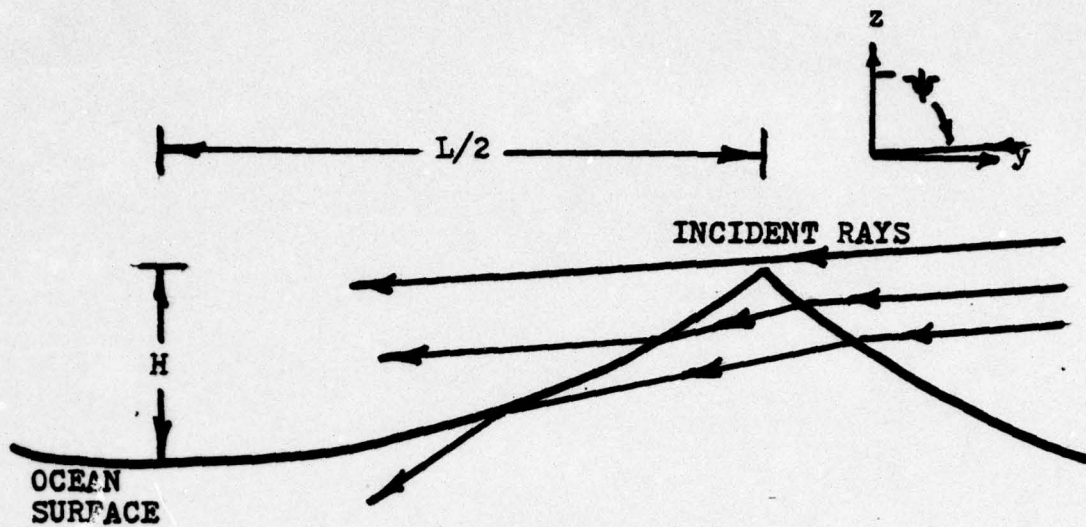


Figure 3: Possible beam paths at high incidence angles

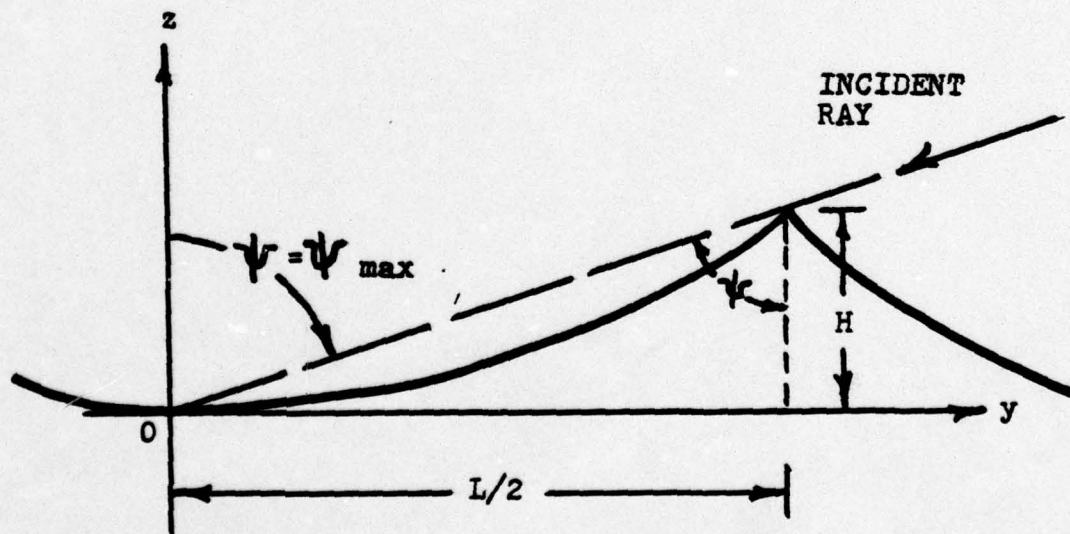


Figure 4: Maximum angle of incidence wave geometry

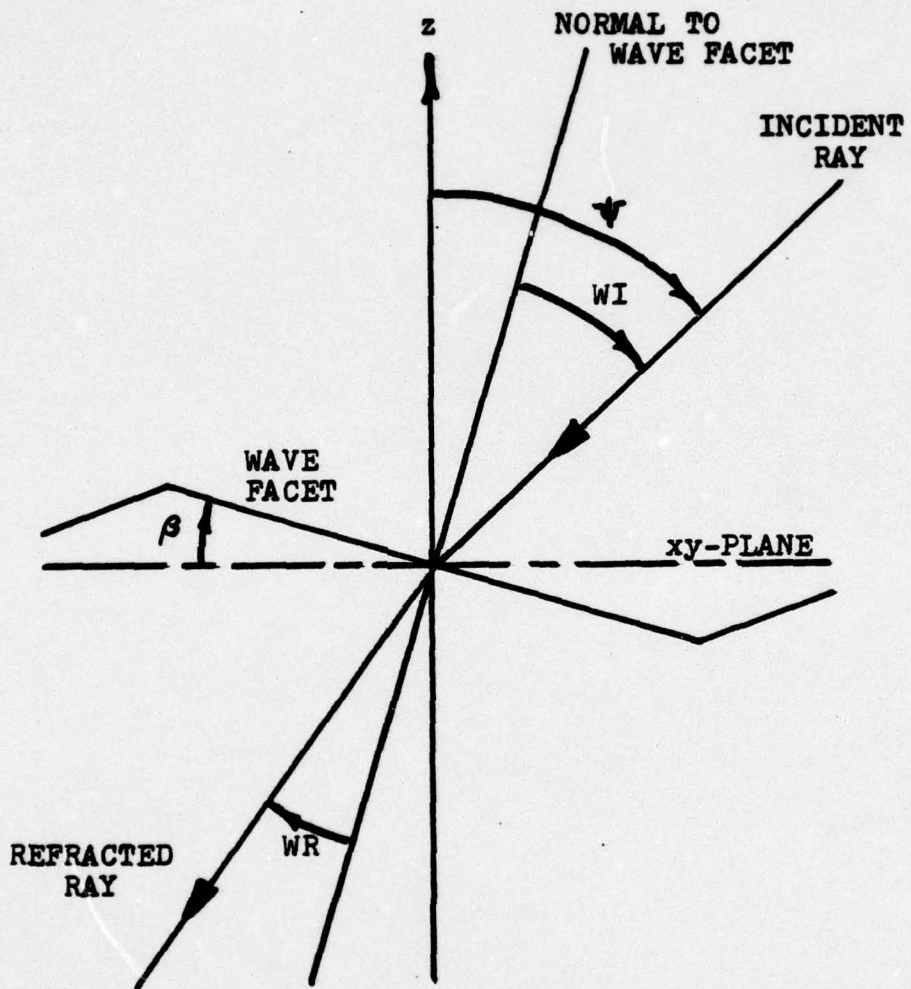


Figure 5: Ray refraction geometry

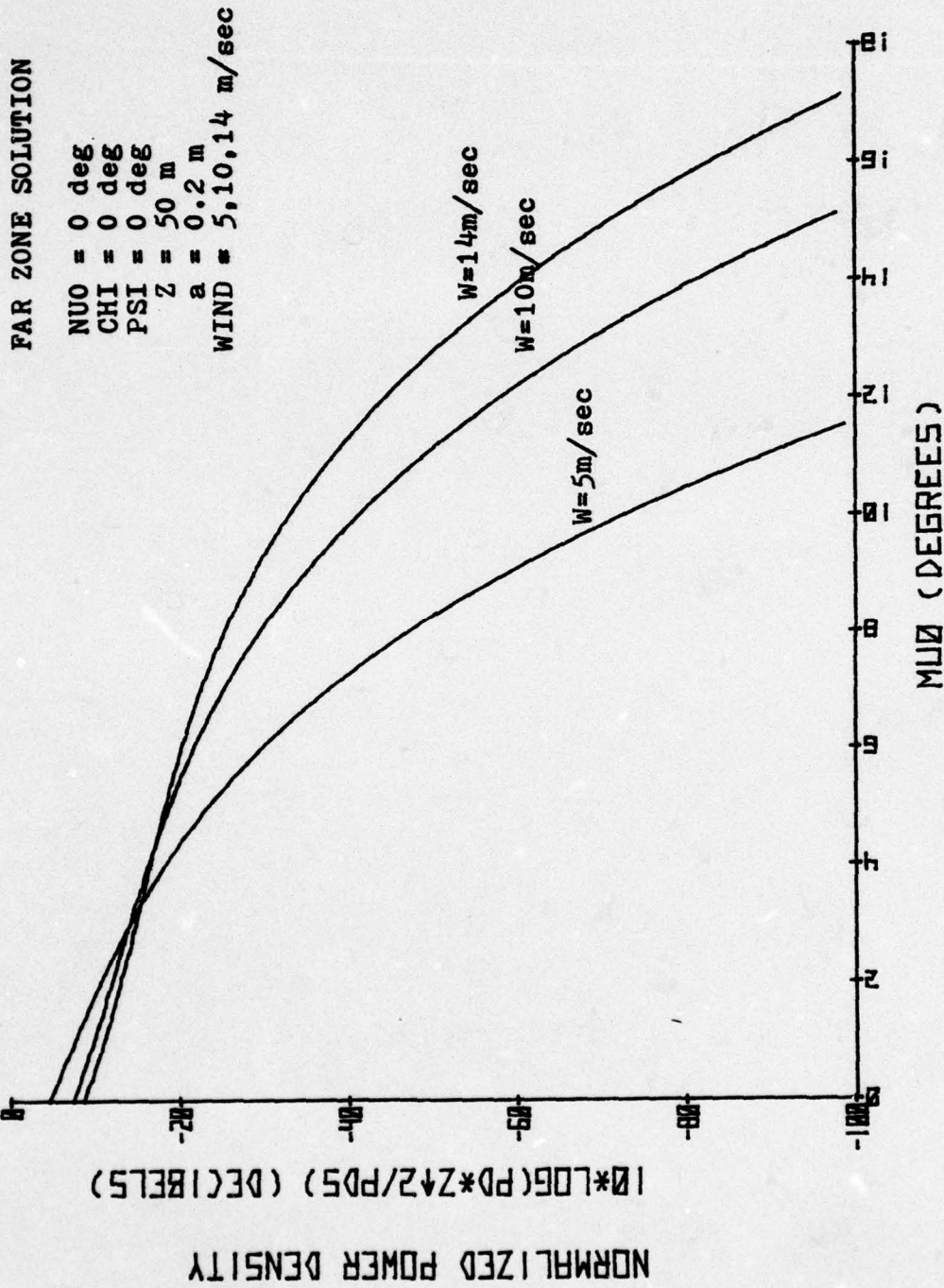


Figure 6

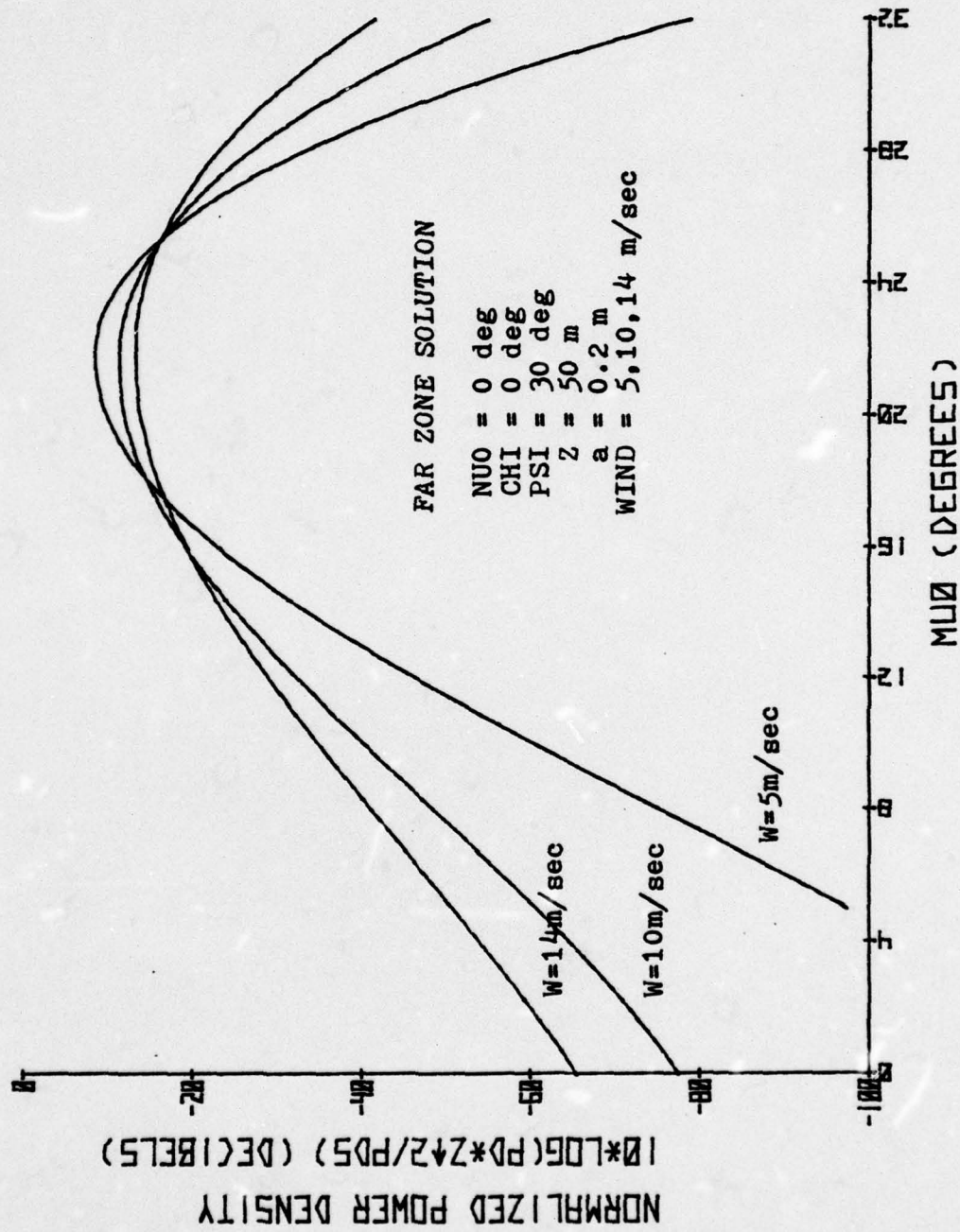


Figure 7

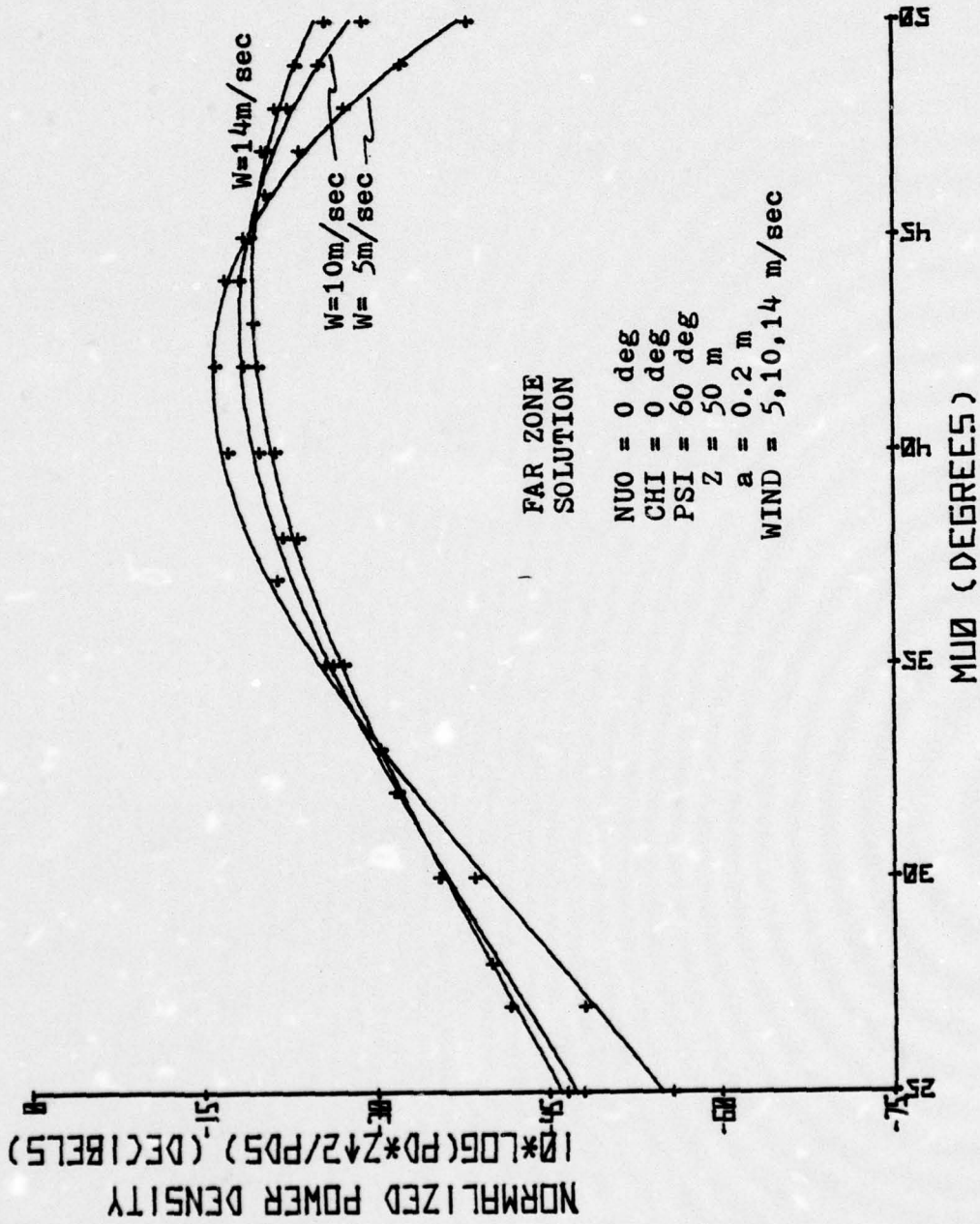


Figure 8

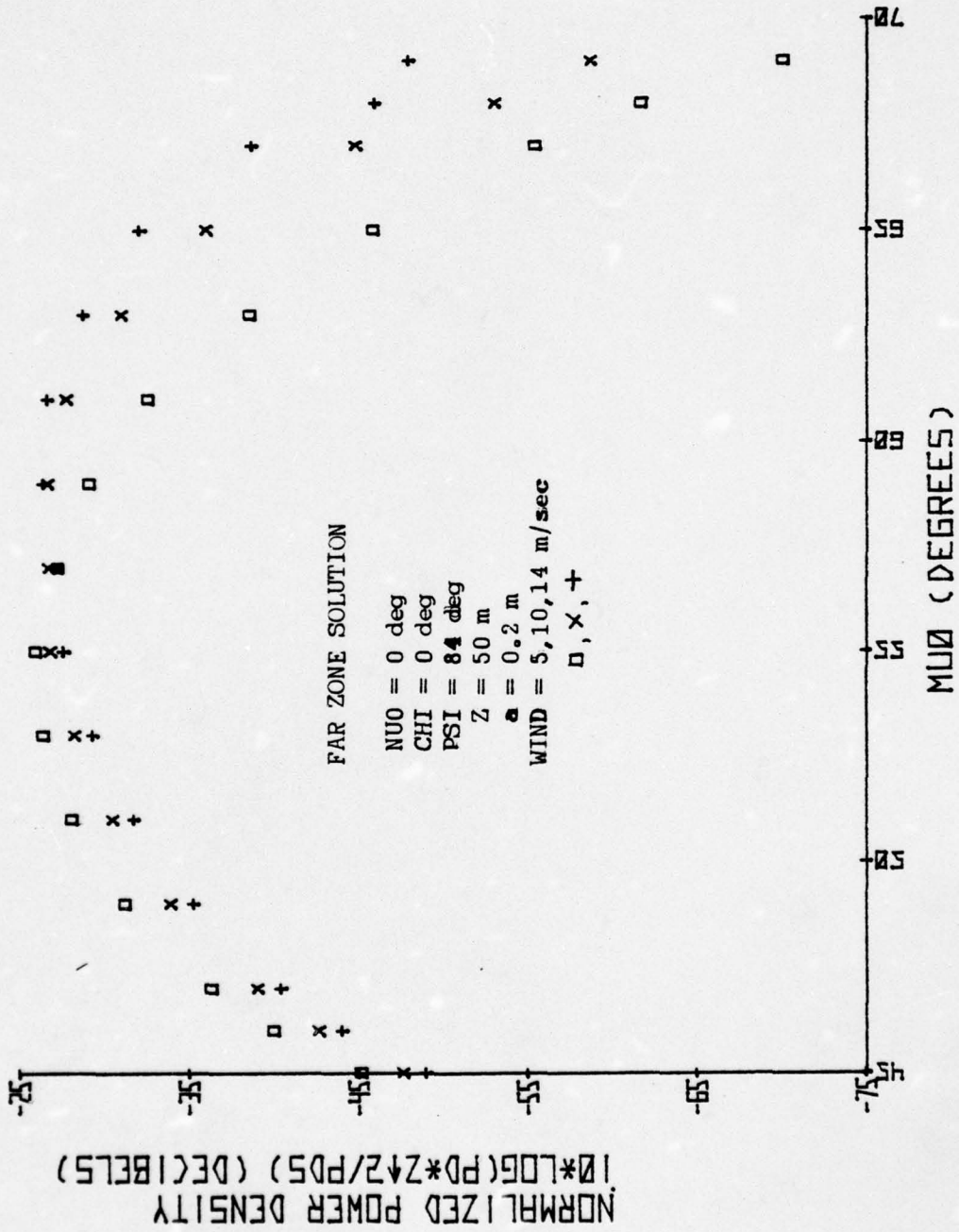


Figure 9

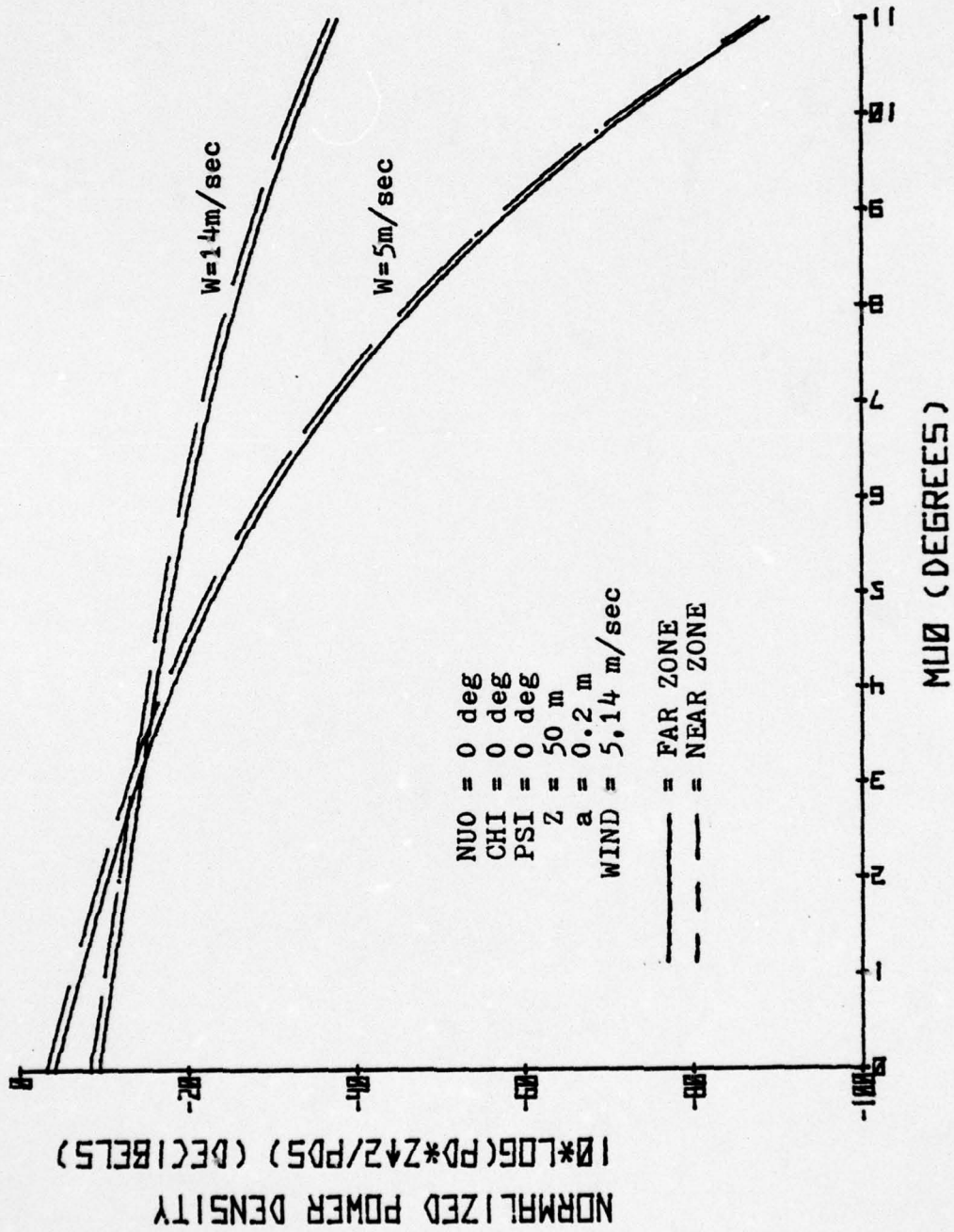


Figure 10

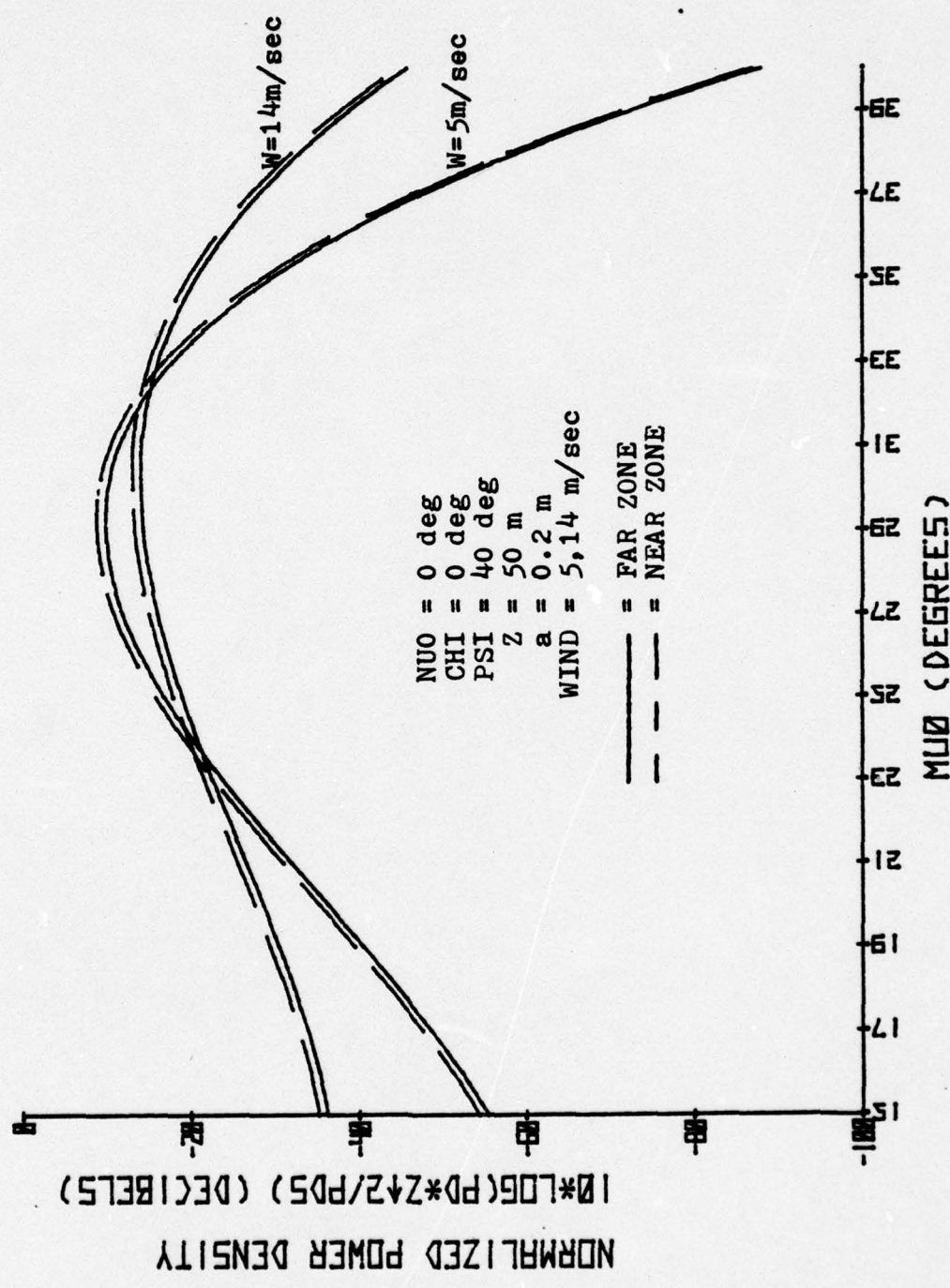


Figure 11

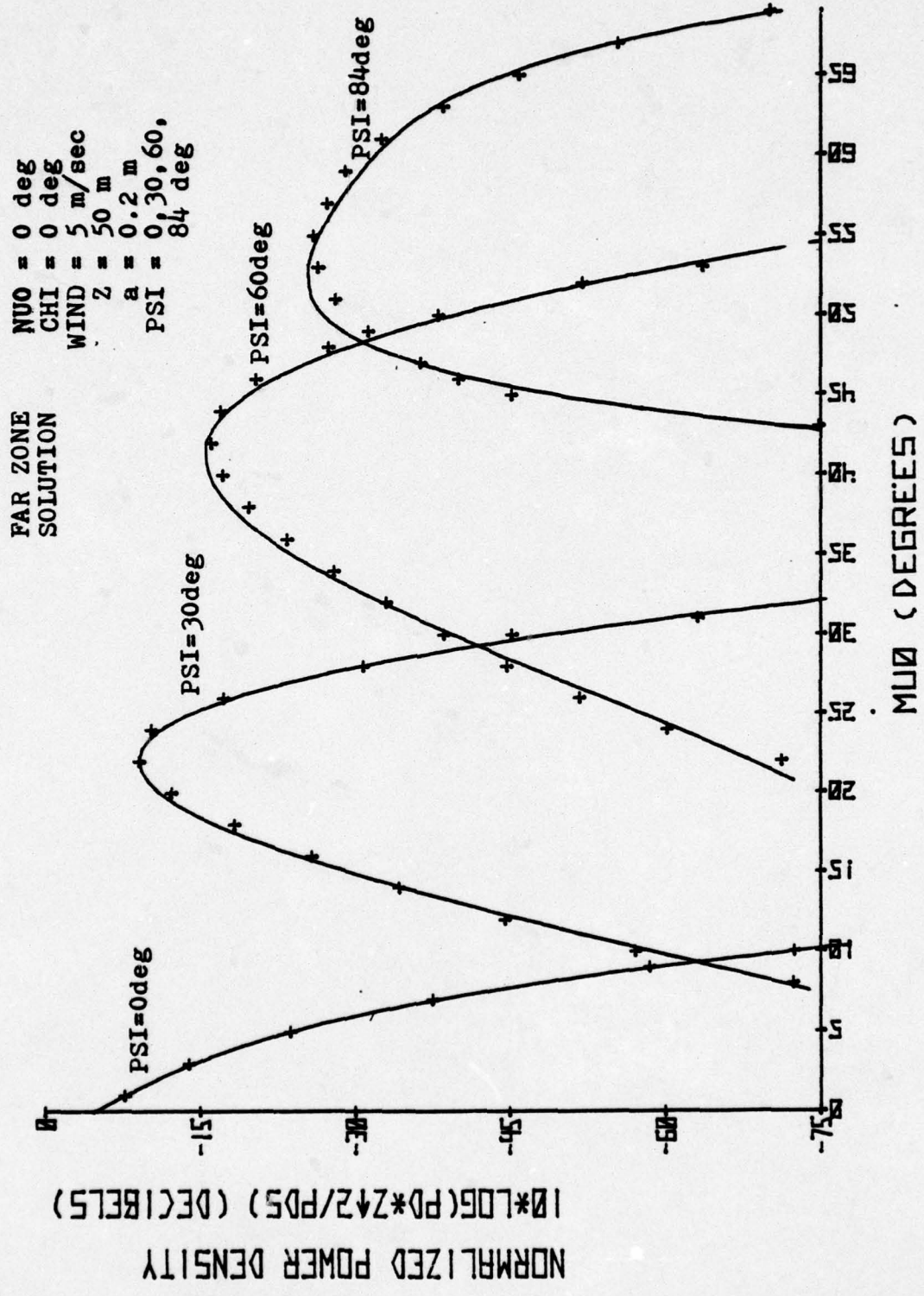


Figure 12

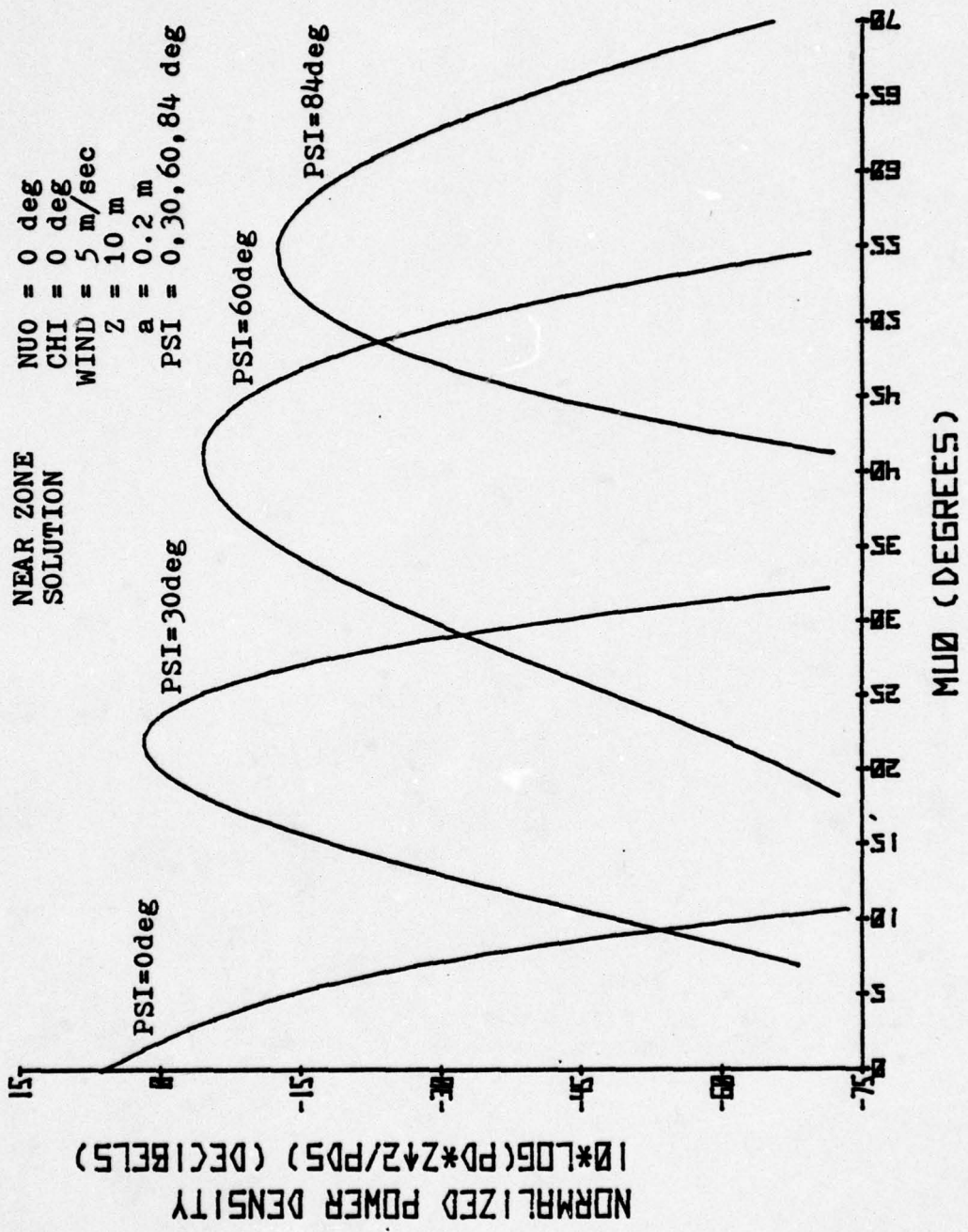


Figure 13

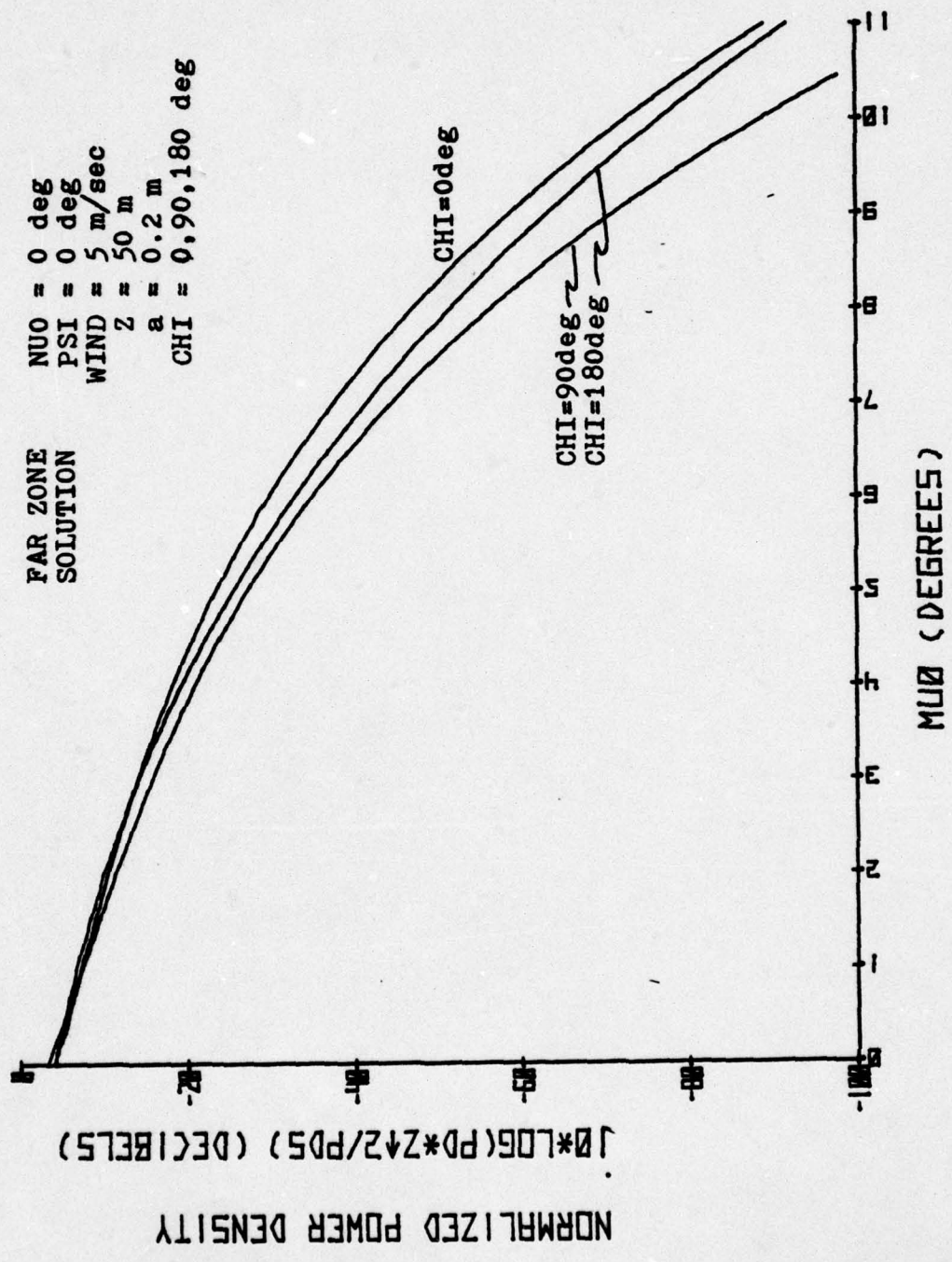


Figure 14

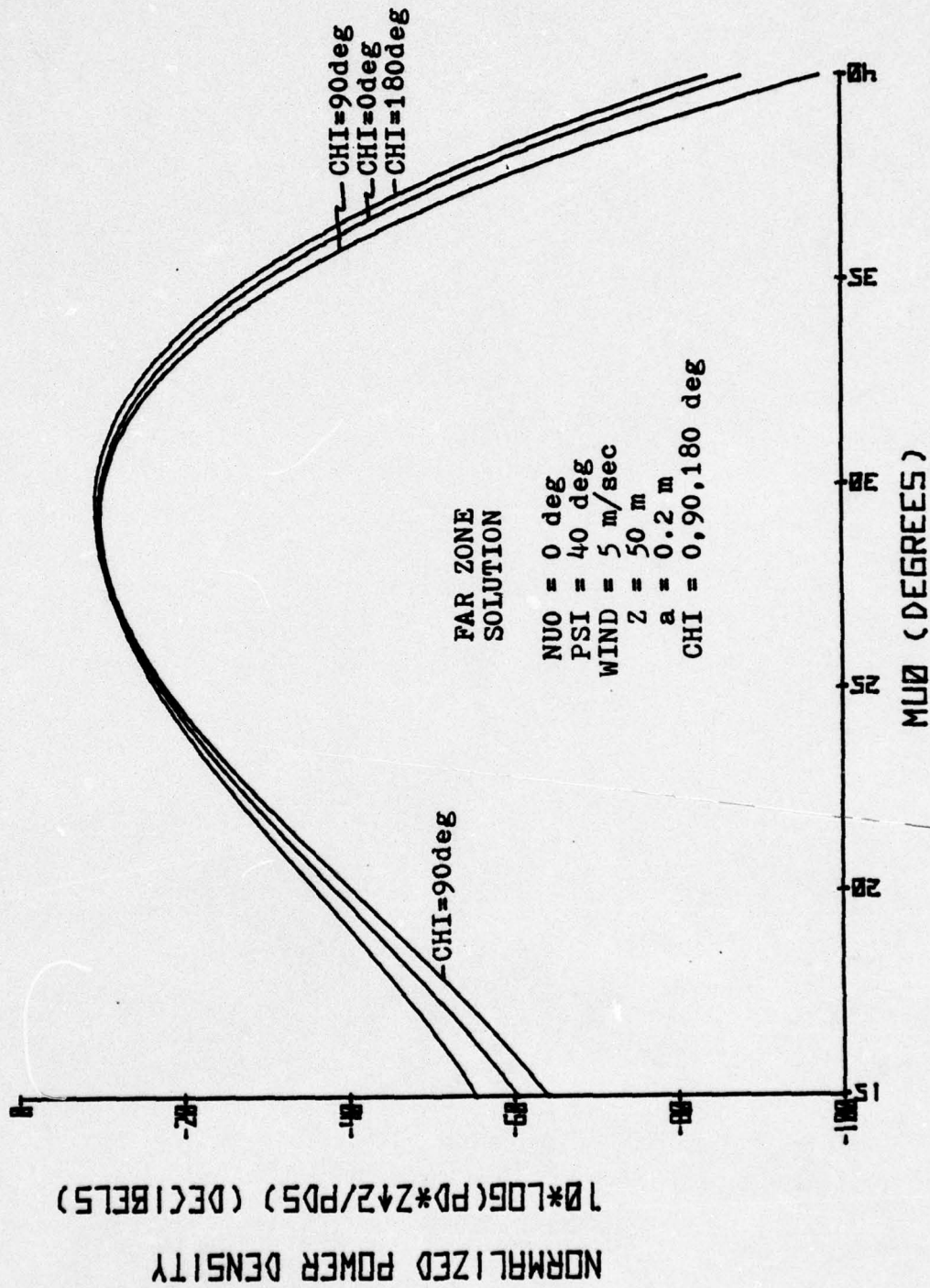


Figure 15

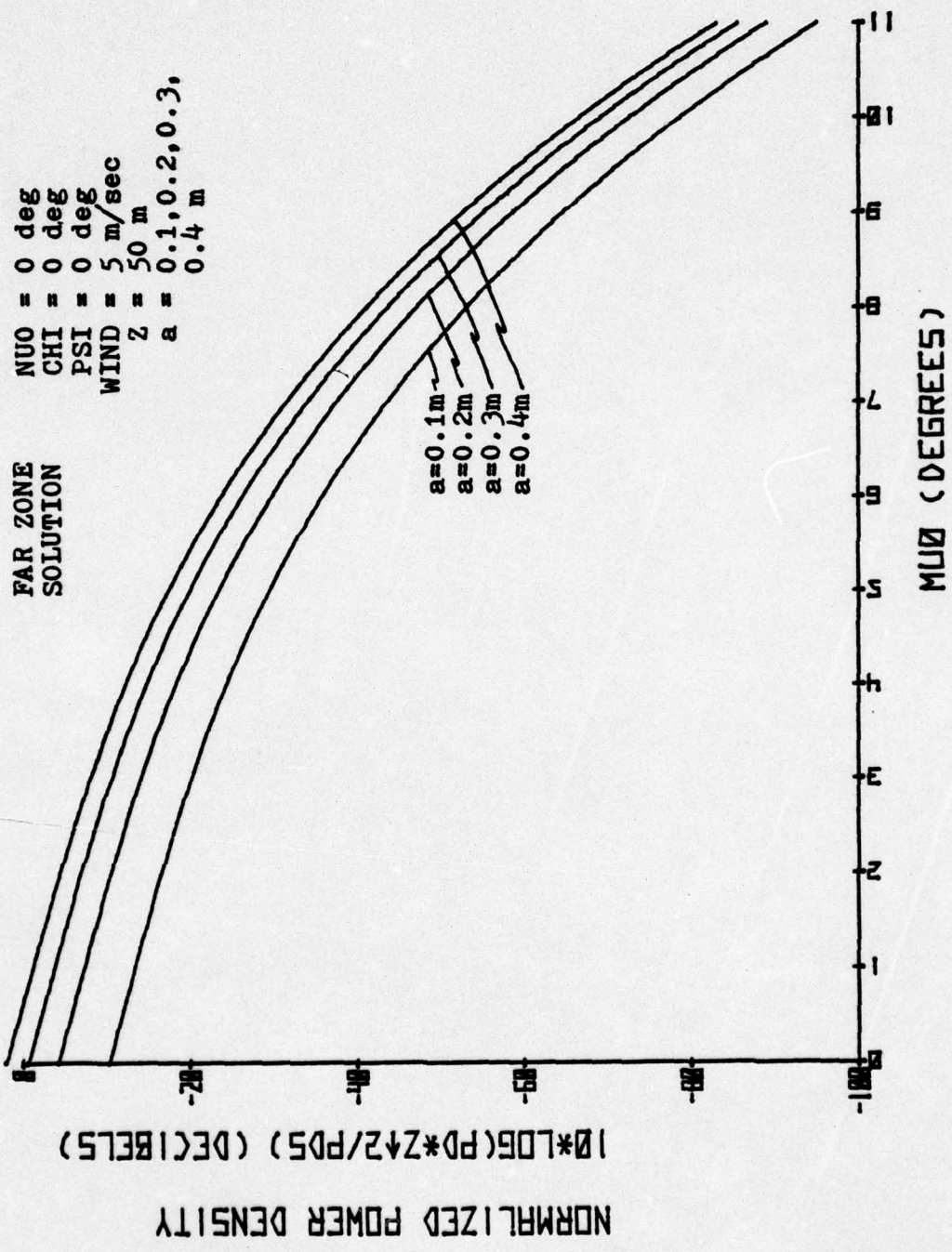


Figure 16

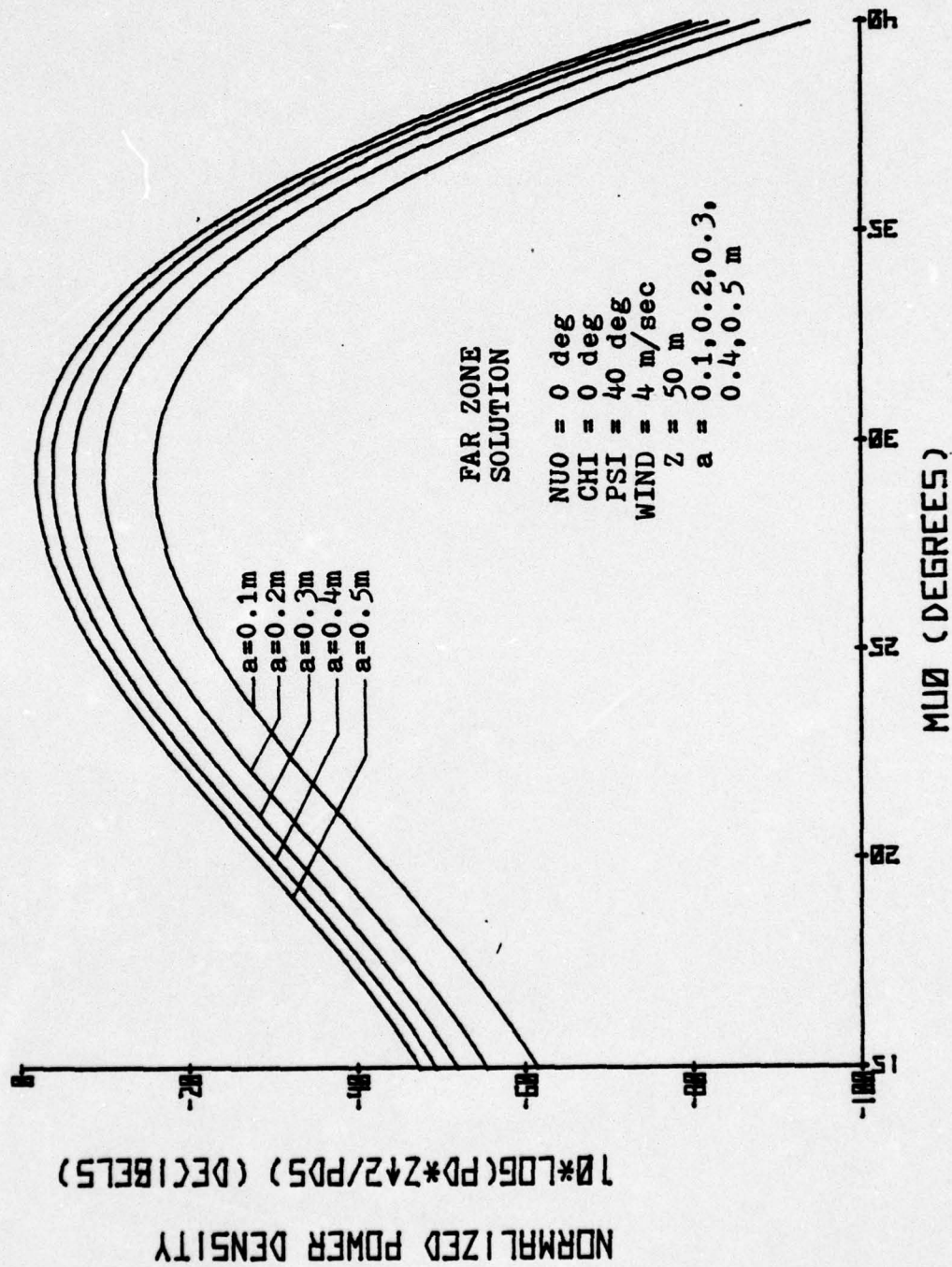


Figure 17

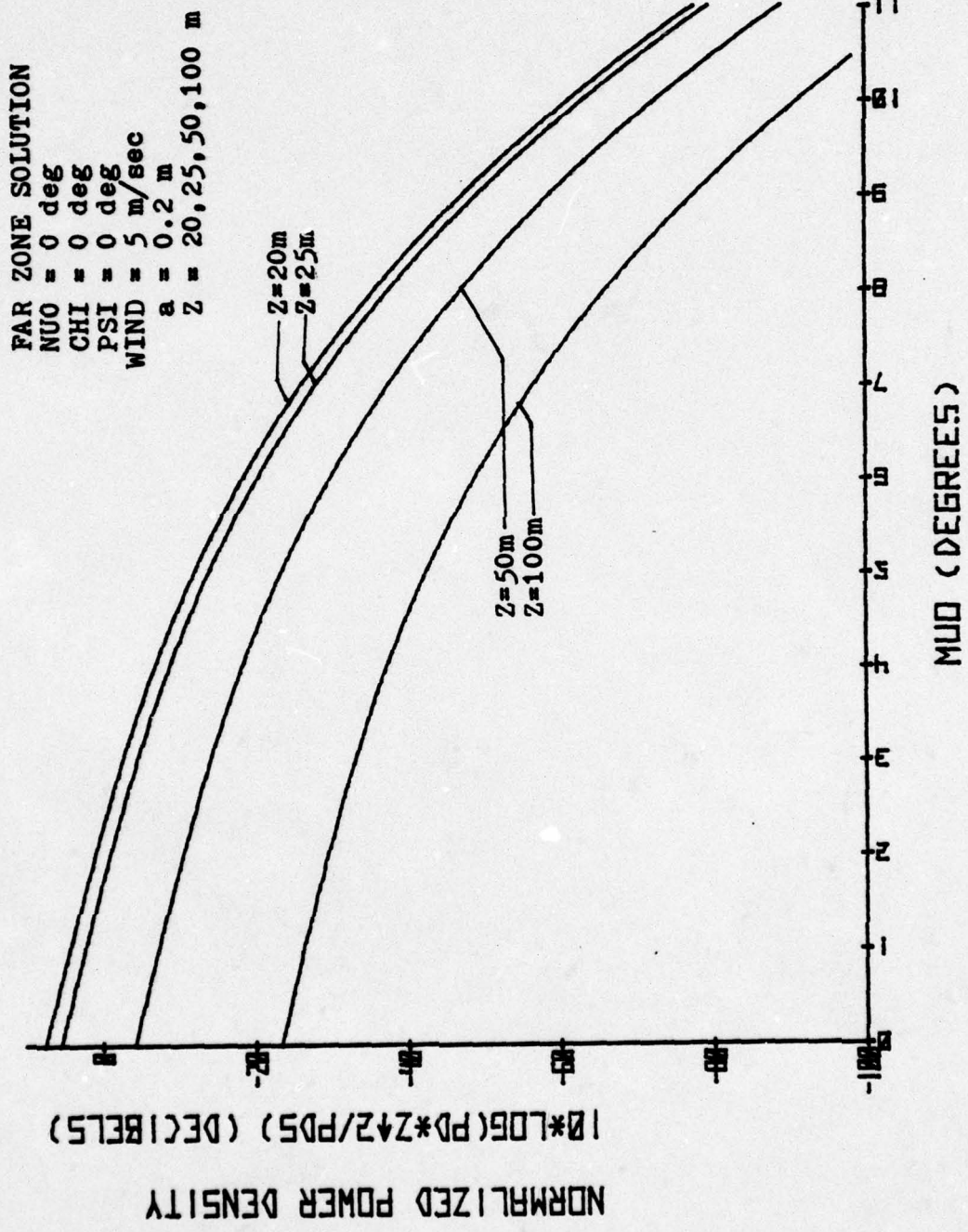


Figure 18

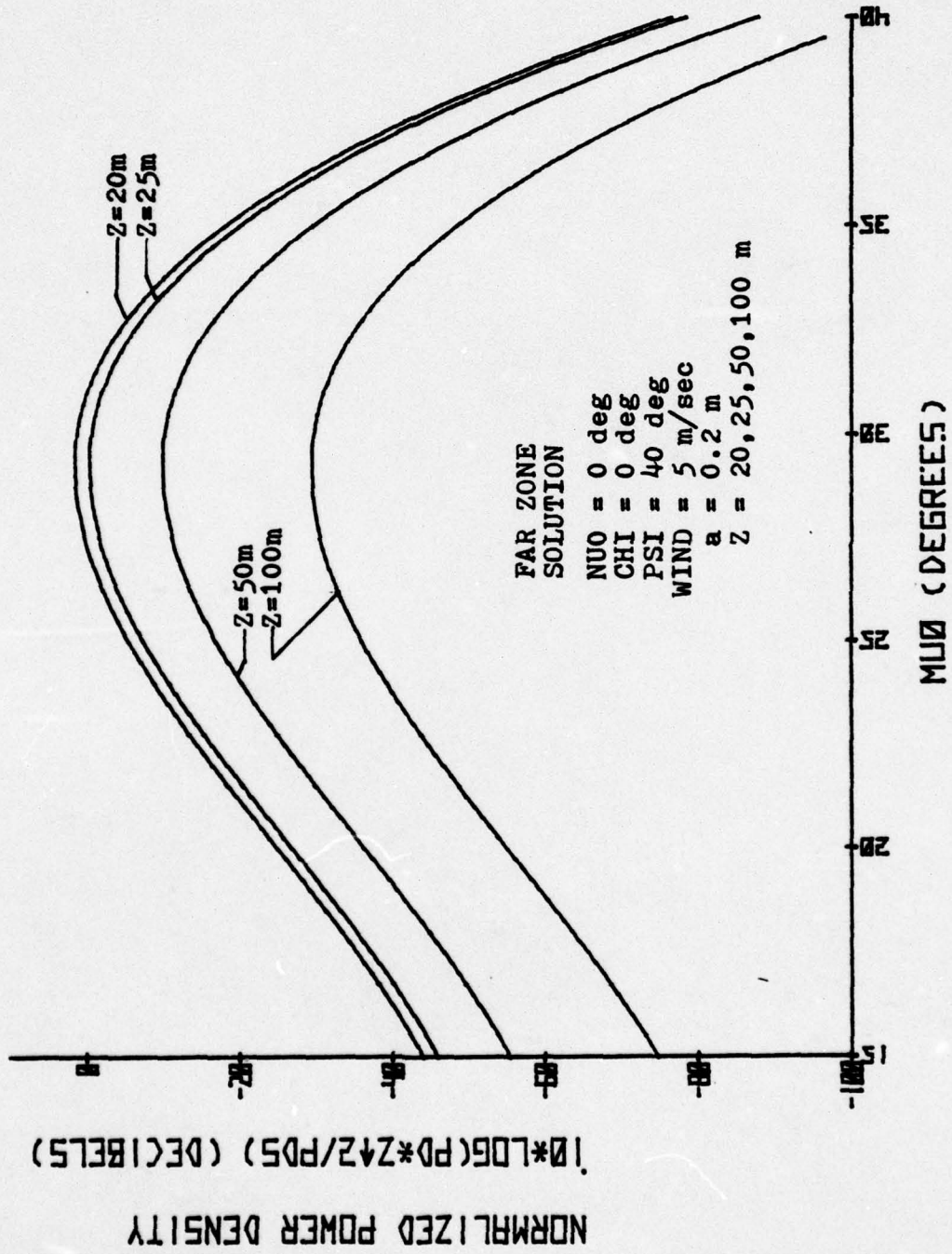


Figure 19

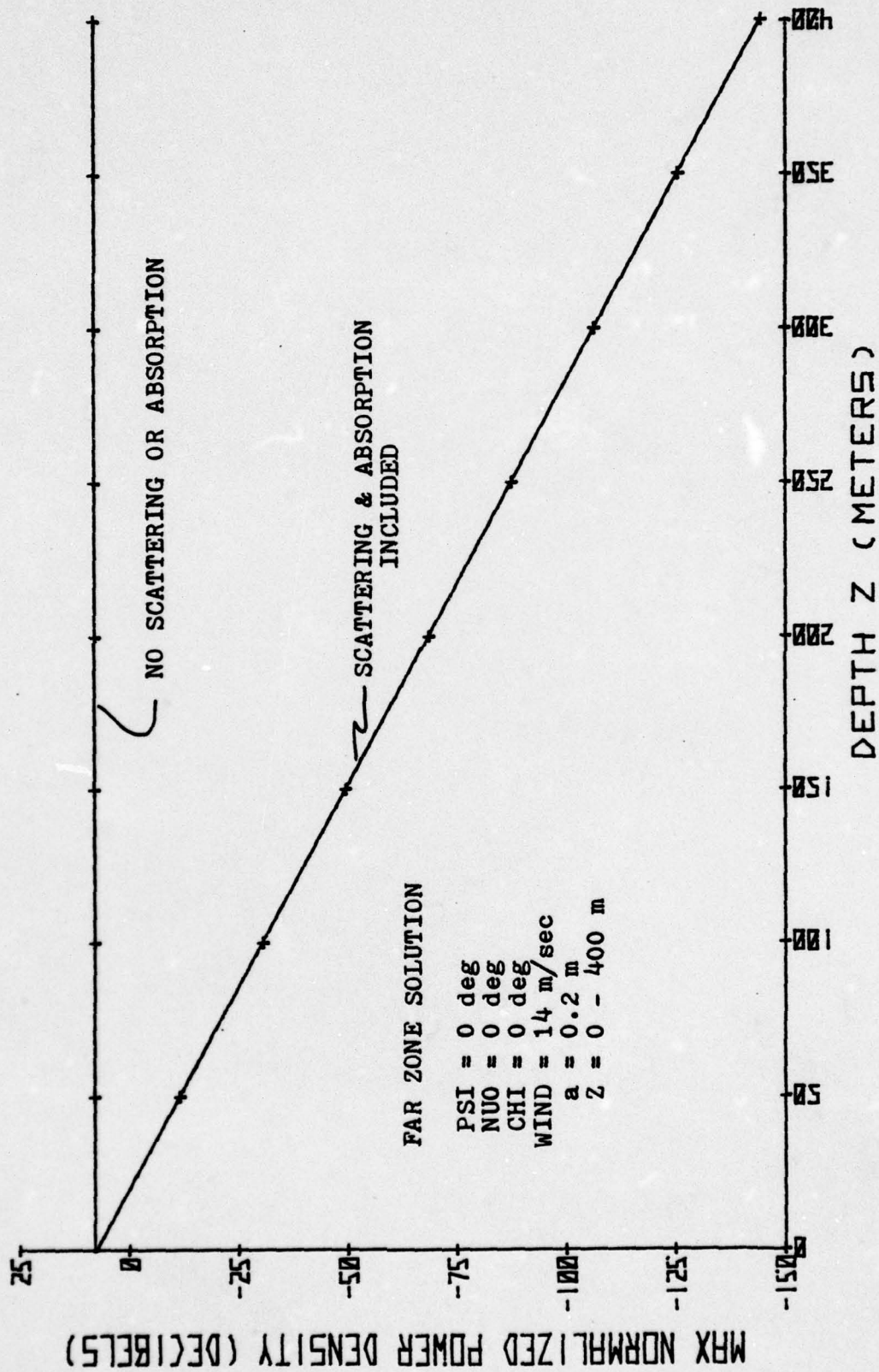


Figure 20

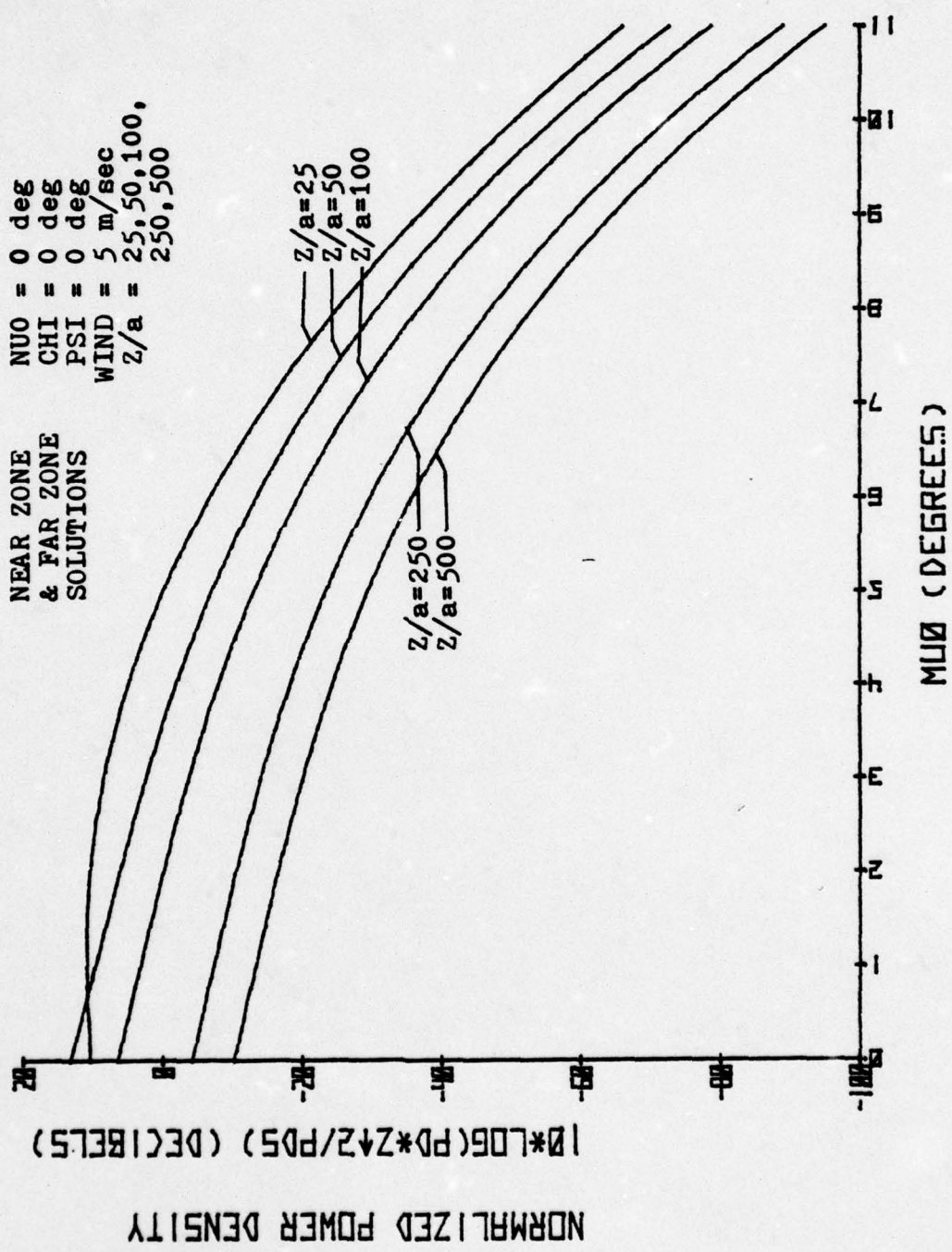


Figure 21

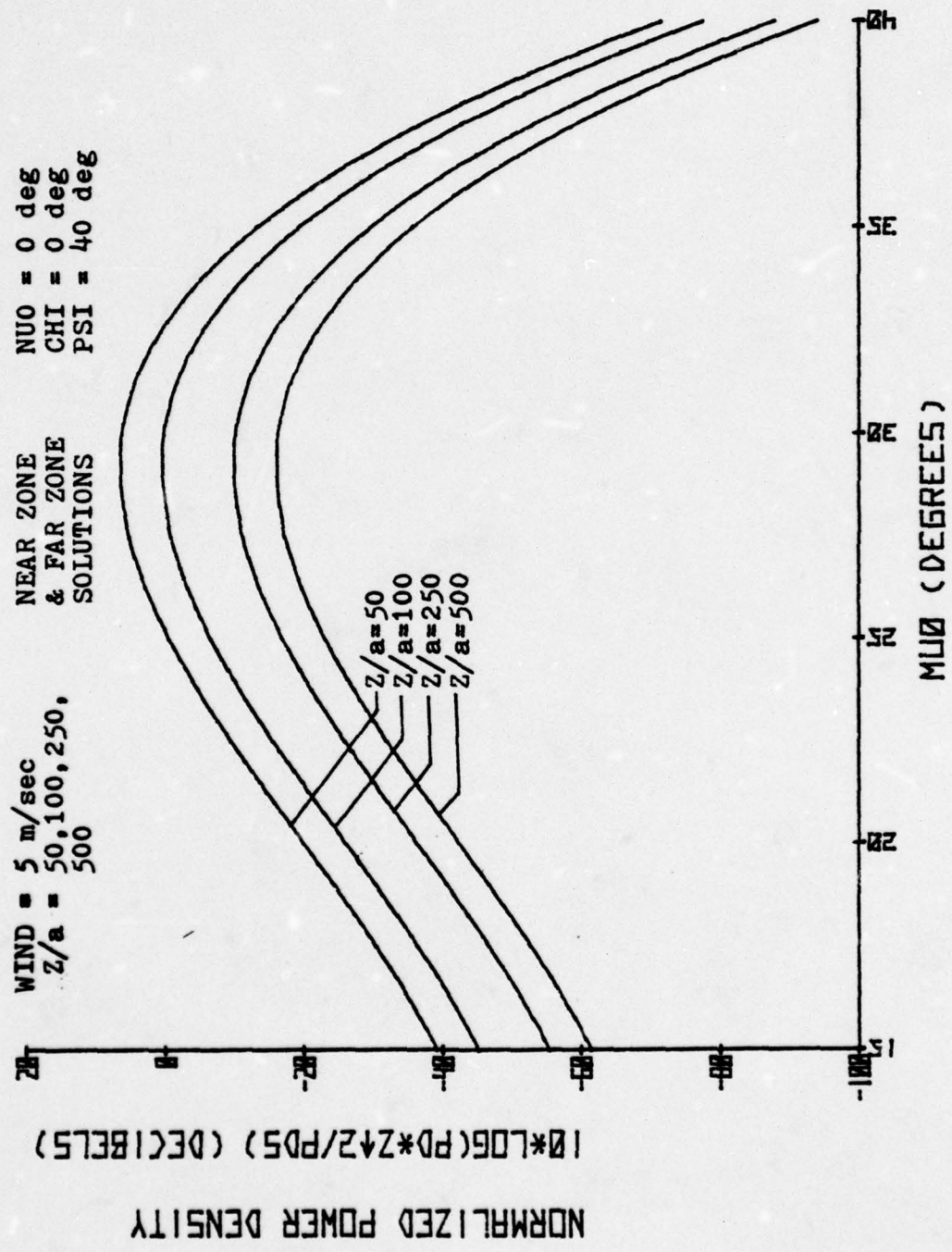


Figure 22

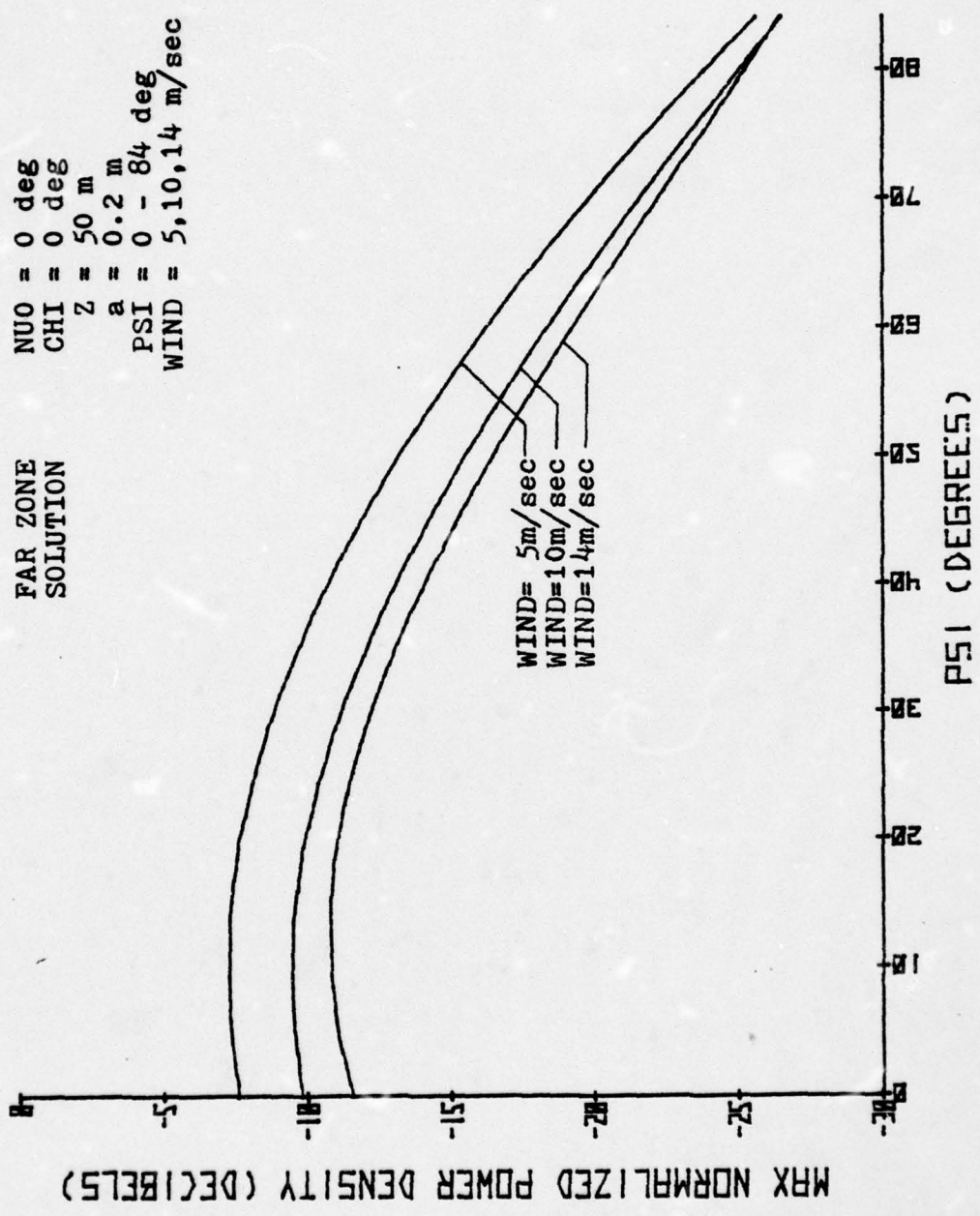


Figure 23

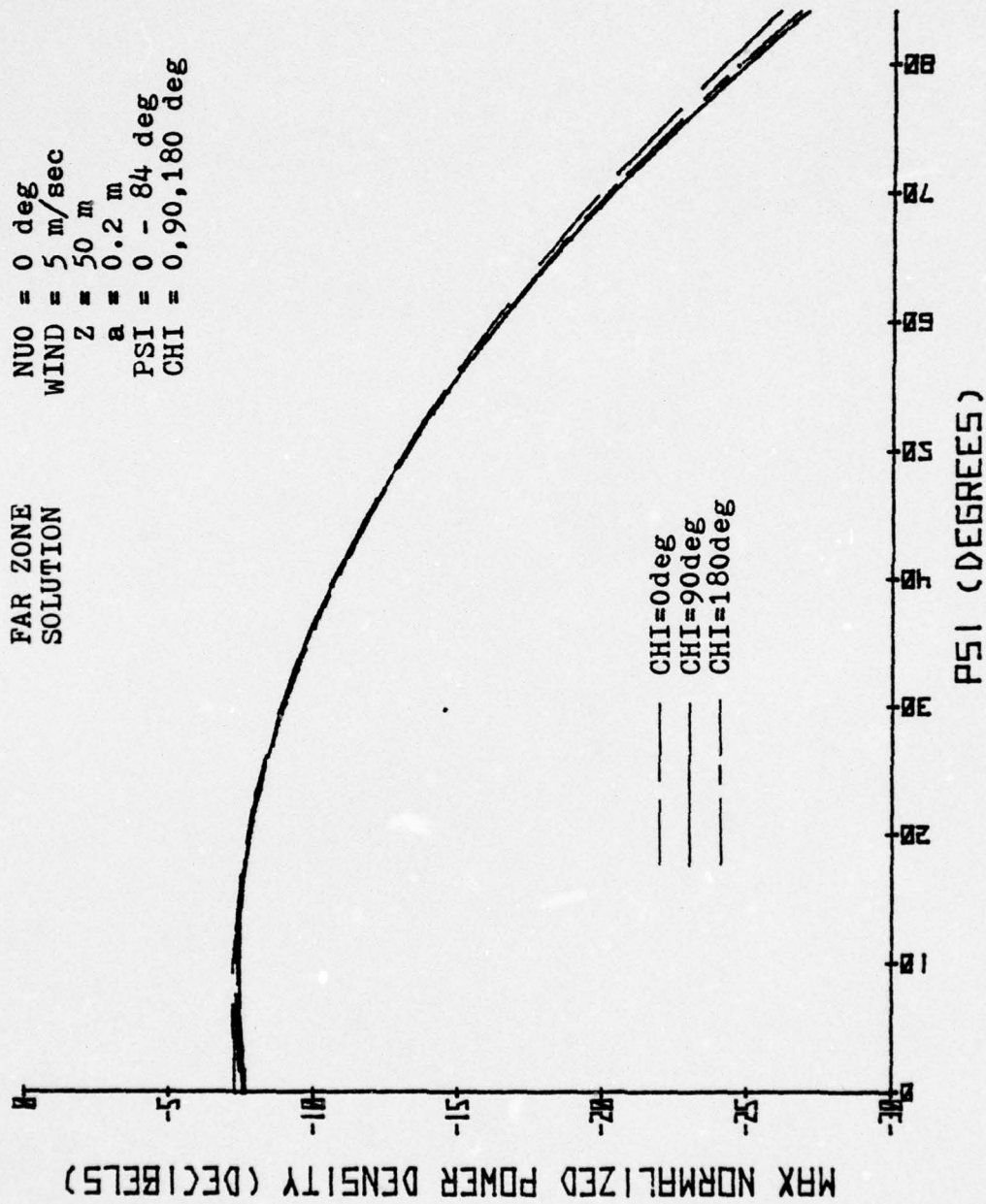


Figure 24

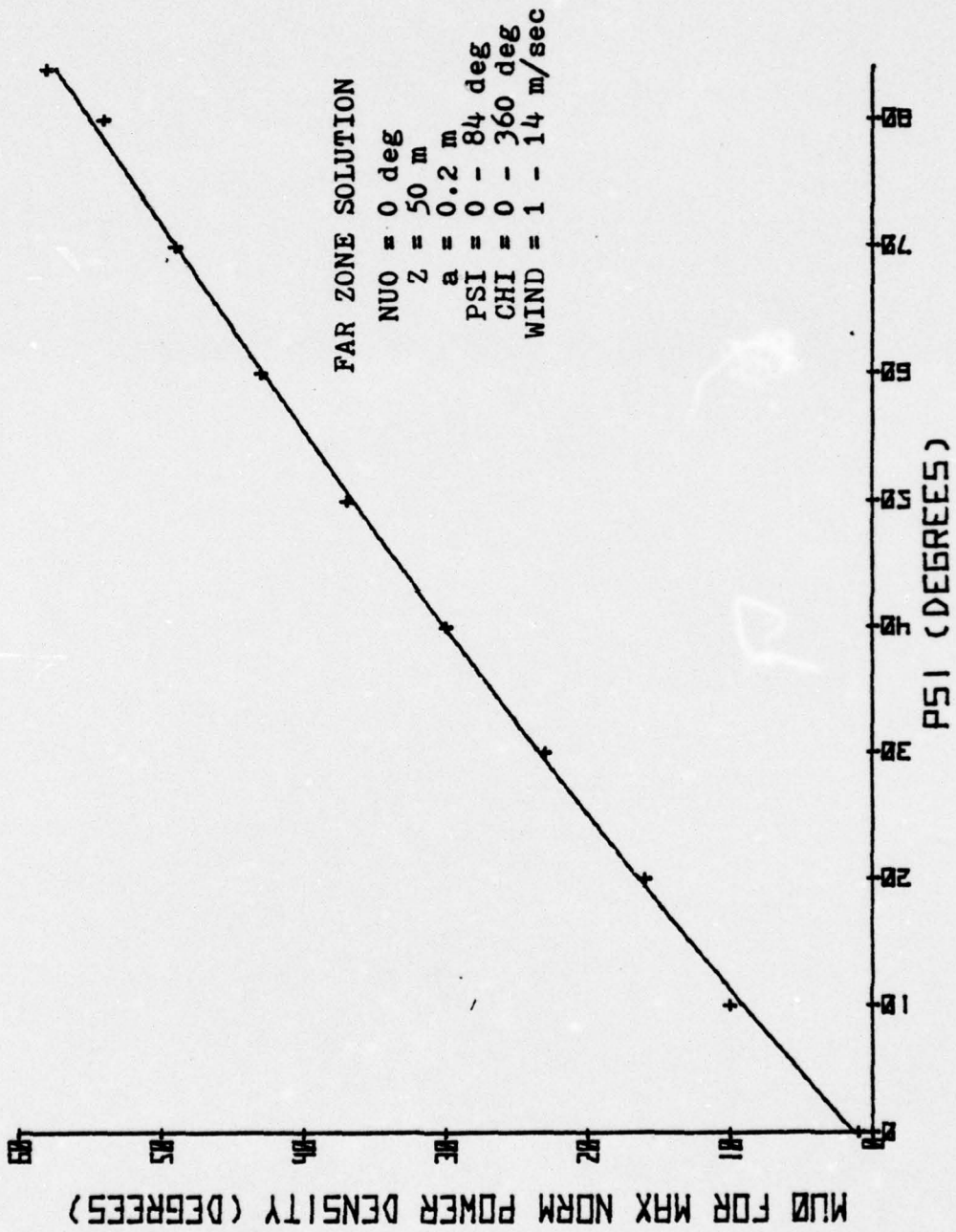


Figure 25

## APPENDIX B

### COMPUTER PROGRAM USAGE

To use the computer programs listed following this Appendix, first compute the ratio of the depth of the point of observation below the ocean surface to the beam radius at the surface facet,  $Z/a$ . Use the Near Zone program for  $Z/a \leq 100$  and the Far Zone program for  $Z/a > 100$ . The Near Zone program may be used for any value of  $Z/a$ , but a slight computation time and computer storage increase will result.

The only other basic requirement is the selection of eight input variables. The variables are listed below along with the line from the respective program in which they appear.

<u>VARIABLE</u>	<u>NEAR</u> <u>ZONE</u>	<u>FAR</u> <u>ZONE</u>
Depth, Z (m)	470	440
Beam radius, RAD (m)	480	450
Angle $Nu_0$ , NUORUN (deg)	490	480
Backward scattering coefficient, BS	560	530
Absorption coefficient, AC ( $m^{-1}$ )	570	540
Beam incidence angle, PSIRUN (deg)	630	590
Wind direction, CHI (rad)	680	640
Wind velocity, W (m/sec)	710	670

Z, RAD, NUORUN, BS and AC are direct program inputs

made on the indicated lines. PSI, CHI and W are selected from DATA statements 430 and 440 in the Near Zone program and 420 and 430 in the Far Zone program. The variable locations in DATA statements were used for multiple variations of the parameters in a slightly different form of the program than presented which is easily set up with DO LOOPS. The entry variables may also be varied in this same manner.

Both programs must be combined with the common package of subroutines that are listed following the basic program listings.

The output from both listed programs appear on the next two pages.

NEAR ZONE COLLUM      DEPTH= 10.00 M      DIF= 2.37845      WIND=14.0 Y/SEC  
 PSI=40.0 DEG      RAD= 0.2 M      VALID=1  
 MUO= 0.0 DEG      CFI= 0.0 DEG      INVAL ID=0

MUO	ALPHA	B	W:	MR	T	JACOB	PSLOPE	PRATIO	PWRDEN	MUO	VALIDITY	XI	ETA
15	0.0	29.93	69.93	44.93	0.2599	0.5512	1.7628E-01	0.5323E-05	-20.69	15	0	0.0	2.7
16	0.0	28.66	66.66	43.66	0.2343	0.4609	1.7189E-01	1.3573E-04	-18.57	16	0	0.0	2.0
17	0.0	24.92	64.92	42.92	0.3320	0.3186	1.207E-01	1.023E-04	-16.56	17	0	0.0	2.0
18	0.0	23.11	63.11	41.11	0.3998	0.2143	5.3529E-01	7.85E-04	-14.56	18	0	0.0	2.0
19	0.0	21.26	61.26	40.26	0.4350	0.2143	6.5461E-01	7.75E-03	-13.50	19	0	0.0	2.0
20	0.0	19.20	59.20	39.20	0.4281	0.1376	9.0402E-01	7.75E-03	-12.50	20	0	0.0	1.1
21	0.0	17.20	57.20	38.20	0.4281	0.1376	1.1544E-01	7.75E-03	-11.50	21	0	0.0	1.1
22	0.0	15.08	55.08	36.08	0.5048	0.0893	1.5497E-01	7.75E-03	-10.50	22	0	0.0	1.1
23	0.0	13.41	53.41	35.41	0.5272	0.0893	2.5231E-01	7.75E-03	-9.50	23	0	0.0	1.1
24	0.0	11.92	51.92	33.92	0.5272	0.0893	3.2691E-01	7.75E-03	-8.50	24	0	0.0	1.1
25	0.0	9.22	45.22	32.22	0.5272	0.0893	4.8954E-01	7.75E-03	-7.50	25	0	0.0	1.1
26	0.0	5.58	42.58	30.58	0.5272	0.0893	6.9488E-01	7.75E-03	-6.50	26	0	0.0	1.1
27	0.0	2.30	39.70	28.70	0.6395	0.0109	9.488E-01	7.75E-03	-5.50	27	0	0.0	1.1
28	0.0	-0.23	36.70	26.70	0.6395	0.0109	1.1057E-01	7.75E-03	-4.50	28	0	0.0	1.1
29	0.0	-3.34	33.58	24.58	0.6395	0.0109	1.8715E-01	7.75E-03	-3.50	29	0	0.0	1.1
30	0.0	-6.72	30.28	22.28	0.6395	0.0109	3.8715E-01	7.75E-03	-2.50	30	0	0.0	1.1
31	0.0	-13.14	26.31	19.31	0.6395	0.0109	7.3345E-01	7.75E-03	-1.50	31	0	0.0	1.1
32	0.0	-20.37	23.03	17.03	0.7008	0.0376	1.8156E-01	7.75E-03	-0.50	32	0	0.0	1.1
33	0.0	-28.15	19.85	14.85	0.7008	0.0376	3.5898E-01	7.75E-03	0.50	33	0	0.0	1.1
34	0.0	-35.97	17.03	12.03	0.7008	0.0376	6.4661E-01	7.75E-03	1.50	34	0	0.0	1.1
35	0.0		14.03	9.03	0.7359	0.0376	1.2004E-01	7.75E-03	2.50	35	0	0.0	1.1
36	0.0		11.03	6.03	0.7359	0.0376	2.2004E-01	7.75E-03	3.50	36	0	0.0	1.1
37	0.0		8.03	3.03	0.7359	0.0376	3.2004E-01	7.75E-03	4.50	37	0	0.0	1.1
38	0.0		5.03	0.03	0.7359	0.0376	4.2004E-01	7.75E-03	5.50	38	0	0.0	1.1
39	0.0		2.03		0.7359	0.0376	5.2004E-01	7.75E-03	6.50	39	0	0.0	1.1

SLP 2.000 SLUT: 71      DTG = 0.01121      WIND=14.0 M/SEC  
 PSI = 0.0      VAL ID = 0  
 MWD = 3.0 DEG      CH = 3.0 DEG      INVAL ID = 0

MWD	ALPHA	W	WT	MR	T	JACOB	DAREA	PSI/PE	PRATTN	PHRDN	MUC	VALIDITY	XI	ETA
15	0.0	29.93	69.93	44.93	0.2599	0.5512	2.2846E-04	1.7628E-01	7.9106E-08	-37.04	15	0	0.0	7.0
16	0.0	28.32	68.32	43.66	0.3143	0.4841	1.9628E-04	3.3785E-01	1.2603E-07	-33.01	17	0	0.0	2.0
17	0.0	26.66	66.66	42.62	0.3423	0.3841	1.8178E-04	5.1207E-01	1.9531E-07	-33.01	18	0	0.0	2.0
18	0.0	25.92	65.92	42.11	0.3698	0.2624	1.6944E-04	5.3525E-01	4.4979E-07	-29.58	19	0	0.0	2.0
20	0.0	23.11	63.11	41.23	0.3975	0.2143	1.5934E-04	6.9464E-01	5.8430E-07	-27.81	20	0	0.0	7.0
21	0.0	19.26	59.26	40.26	0.4251	0.1730	1.4818E-04	9.0404E-01	6.3324E-06	-26.66	21	0	0.0	1.0
22	0.0	17.26	57.26	39.07	0.4521	0.1375	1.3892E-04	1.1812E-00	7.4350E-06	-26.66	22	0	0.0	1.0
23	0.0	15.64	55.64	38.07	0.4788	0.1013	1.3028E-04	1.5474E-00	8.1231E-06	-26.66	23	0	0.0	1.0
24	0.0	12.78	52.78	37.41	0.5048	0.0813	1.2208E-04	2.0977E-00	8.9070E-06	-26.66	24	0	0.0	1.0
25	0.0	10.41	50.41	37.09	0.5300	0.0592	1.1508E-04	3.2231E-00	9.4183E-06	-26.66	25	0	0.0	1.0
26	0.0	7.62	47.62	36.52	0.5542	0.0433	1.0816E-04	4.8914E-00	9.9994E-06	-26.66	26	0	0.0	7.0
27	0.0	5.32	45.32	36.28	0.5775	0.0242	1.0174E-04	7.2914E-00	1.0598E-05	-26.66	27	0	0.0	2.0
28	0.0	2.58	42.58	36.07	0.6202	0.0105	9.5727E-05	1.0485E-00	1.2062E-05	-26.66	28	0	0.0	0.0
29	0.0	-3.20	39.72	35.71	0.6395	0.0019	9.0677E-05	1.4460E-00	1.4460E-05	-26.66	29	0	0.0	0.0
30	0.0	-6.42	36.56	35.26	0.6573	0.0192	8.5383E-05	1.9488E-00	1.4460E-05	-26.66	30	0	0.0	0.0
31	0.0	-9.74	33.56	34.86	0.6735	0.0262	8.0105E-05	2.6175E-00	1.3788E-05	-26.66	31	0	0.0	0.0
32	0.0	-13.14	30.28	34.31	0.6880	0.0322	7.5110E-05	3.5155E-00	1.3244E-05	-26.66	32	0	0.0	0.0
33	0.0	-16.67	26.86	33.71	0.7078	0.0376	7.0155E-05	4.8155E-00	1.2866E-05	-26.66	33	0	0.0	0.0
34	0.0	-20.31	23.31	33.13	0.7117	0.0422	6.5288E-05	6.5288E-01	1.2555E-05	-26.66	34	0	0.0	0.0
35	0.0	-24.07	19.63	32.53	0.7207	0.0463	6.0490E-05	9.1675E-01	1.2061E-05	-26.66	35	0	0.0	0.0
36	0.0	-28.02	15.98	31.93	0.7277	0.0503	5.5806E-05	1.2671E-01	1.1050E-05	-26.66	36	0	0.0	0.0
37	0.0	-31.69	12.49	31.34	0.7328	0.0548	5.1293E-05	1.7671E-01	1.0050E-05	-26.66	37	0	0.0	0.0
38	0.0	-35.19	8.03	30.78	0.7359	0.0578	4.6743E-05	2.2904E-01	9.7785E-05	-26.66	38	0	0.0	0.0

NEAR ZONE COMPUTER PROGRAM

10  
20  
30  
40  
50  
60  
70  
80  
90  
100  
110  
120  
130  
140  
150  
160  
170  
180  
190  
200  
210  
220  
230  
240  
250  
260  
270  
280  
290  
300  
310  
320  
330  
340  
350  
360  
370  
380  
390  
400  
410  
420  
430  
440  
450  
460  
470  
480

NEAR ZONE SOLUTION OF THE TIME-AVERAGE POWER PROBABILITY  
DISTRIBUTION BELOW THE OCEAN OF A LASER BEAM INCIDENT ON SURFACE

NCMENCLATURE:

PSI=ANGLE OF INCIDENT BEAM WITH RESPECT TO VERTICAL AXIS  
CHI=ANGLE OF WIND WITH RESPECT TO THE INCIDENT BEAM IN  
THE XY-PLANE  
ALPHA=ANGLE OF MAX WAVE SLOPE WITH RESPECT TO THE INCIDENT  
BEAM IN THE XY-PLANE  
B=MAX SLOPE OF WAVE FACET  
NU=NUO=ANGLE BETWEEN REFRACTED RAY PROJECTED ONTO XY-PLANE  
AND THE Y AXIS  
MU=MUO=ANGLE BETWEEN REFLECTED RAY AND THE Z AXIS  
Z=DEPTH BELOW OCEAN SURFACE (METERS)  
RAD=INCIDENT RAY SPOT RADIUS AT WAVE FACET (MINOR AXIS OF  
ELLIPSE WHEN PSI IS NON-ZERO)  
BB=MAJOR AXIS OF SPOT INCIDENT ON WAVE FACET  
WI=WIND VELOCITY (M/SEC)  
WI=RAY INCIDENCE ANGLE  
WR=RAY REFRACTION ANGLE  
LTF=DIFFUSE TRANSMITTANCE FUNCTION  
BS=BACKWARD SCATTERING COEFFICIENT  
AC=ABSORPTION COEFFICIENT  
T=FRSNEL'S TRANSMITTANCE FUNCTION  
AN=INDEX OF REFRACTION  
PSLOPE=SLOPE PROBABILITY FUNCTION  
DAREA=AREA INCREMENT  
JACOB=JACOBIAN  
PWRDEN=POWER DENSITY (DECIBELS)

INTEGER VALID  
REAL NUO, JMUC, JACOB, MUO, NUORUN  
REAL MUU, MUL, NUU, NUL  
COMMON MUO, NUO, PSI, AN, PSIRUN, NUORUN, PI, Z, RAC, BB, JK  
DIMENSION W(4), CHI(3), NCHI(3), RG(4), JMUC(90), PWRDEN(90), PSIN  
1(110)

INPUT PARAMETERS FOR THIS RUN

DATA W, CHI, NCHI/14, 10, 5, 1, 0, 1, 5708, 3, 14159, 0, 90, 180/  
DATA PSIN/0, 10, 20, 30, 40, 50, 60, 70, 80, 84/  
DATA ETAL, ETAL2, XI1, XI2/.577350269, -.577350269, .577350269, -.577350269  
165/  
Z = 10.  
RAD = .2

CCCCCCCCCCCCCCCCCCCCCCCCCCCCCCCCCCCC

CC



```

C 120 INT = 15
C 125 CC 195 J=INT,90
      JMU0(J) = FLOAT(J)
      MLC = JMU0(J)/57.2958
      JK = J
      JJ = J-6
C ALPHA,B,WI,WR ARE COMPUTED IN SUBROUTINE ANGLES:
C CALL ANGLS (ALPHA,B,WI,WR)
C REFS 2,3&4
C T=FRESNEL'S TRANSMITTANCE
C REFS 9&10
C TPER = (2.*COS(WI)*SIN(WR)/SIN(WI+WR))**2
C TPAR = (2.*COS(WI)*SIN(WR)/SIN(WI+WR))*COS(WI-WR)**2
C T = (TPAR+TPER)/2.
C JACCBIAN COMPUTED IN SUBROUTINE JACO
C CALL JACO (ALPHA,B,JACCB)
C REF 3: EQNS 48-52
C PSLCPE=SLOPE 5-9;12-18
C REFS 5: EQNS 1.003+1.92E-03*W(I)
C SIGU = SQRT(3.16E-03*W(I))
C C01 = .01-.0086*W(I)
C C03 = .04-.033*W(I)
C C4C = .4
C C22 = .12
C C24 = .23
C AP = ALPHA-CHI(L)
C ZXP = ATAN(B)*SIN(AP)
C ZYP = TAN(B)*COS(AP)
C XI = ZXP/SIGU
C ETA = ZYP/SIGU
C FACT1 = (1./2.*PI*SIGC*SIGU))*EXP(-.5*(XI**2+ETA**2))
C FACT2 = 1./5*C21*(XI**2-1.)*ETA-(1./6.)*C03*(ETA**3-3.*ETA)
C FACT3 = (1./24.)*C40*(XI**4-6.*XI**2+3.)*+.25*C22*(XI**2-1.)*(ETA**
12-1.)
C FACT4 = (1./24.)*C04*(ETA**4-6.*ETA**2+3.)
C FLSLOPE = FACT1*(FACT2+FACT3+FACT4)
C VALIDITY CHECK (VALID=1; INVALID=0) ON SLCPE PROBABILITY
C AXI = ABS(XI)
C AETA = ABS(ETA)
C VALID = 1
C IF ((AXI.GT.2.5).OR.(AETA.GT.2.5)) VALID=0

```

```

570
980
990
1000
1010
1020
1030
1040
1050
1060
1070
1080
1090
1100
1110
1120
1130
1140
1150
1160
1170
1180
1190
1200
1210
1220
1230
1240
1250
1260
1270
1280
1290
1300
1310
1320
1330
1340
1350
1360
1370
1380
1390
1400
1410
1420
1430
1440

```



1930  
1940  
1950  
1960  
1970  
1980  
1990  
2000  
2010  
2020  
2030  
2040  
2050  
2060  
2070  
2080  
2090  
2100  
2110  
2120  
2130  
2140  
2150  
2160  
2170  
2180  
2190  
2200  
2210  
2220  
2230  
2240  
2250  
2260  
2270  
2280  
2290  
2300  
2310  
2320  
2330  
2340  
2350  
2360  
2370  
2380  
2390  
2400

```

CE = SQRT(BB**2*CTNU**2-(BB**2/RAD**2)*(Y1**2-8B**2+X1*CTNU*(X1*CT
1A L-2.*Y1)))
1A L-2.*Y1)))
CC = CTNU**2+BB**2/RAD**2
X4 = (CA-(SIN(NUO))/ABS(SIN(NUO)))*CB)/CC
X5 = (CA+(SIN(NUO))/ABS(SIN(NUO)))*CB)/CC
YY4 = BB*SQRT(1.-X4**2/RAD**2)
YY5 = (X4-X1)*CTNU+Y1
Y4 = SIGN(YY4,Y4SG)
YY5 = BB*SQRT(1.-X5**2/RAD**2)
YY5SG = (X5-X1)*CTNU+Y1
Y5 = SIGN(YY5,Y5SG)
GC TO 165

```

C 155 NORMAL INCIDENCE, OUTSIDE BEAM:

```

X1 = 0
X21 = -Z*TAN(MUO)
X221 = -(RAD*SQRT(Y1**2-RAD**2)/Y1)
Y21 = -X21
Y22 = -RAD*SQRT(1.-X21**2/RAD**2)
IF (NUO.NE.0.) GO TO 160
X4 = 0
X5 = 0
Y4 = 0
Y5 = -RAD
GC TO 165

```

16C

```

CTNU = COTAN(NUO)
CNA = -Y1*CTNU**2*CTNU**2-Y1**2+RAD**2)
CNB = SQRT(RAD**2+1.
CNC = CTNU**2+1.
X4 = (CNA-(SIN(NUO))/ABS(SIN(NUO)))*CNC)/CNC
X5 = (CNA+(SIN(NUO))/ABS(SIN(NUO)))*CNC)/CNC
YY4 = BB*SQRT(1.-X4**2/RAD**2)
YY4SGN = X4*CTNU+Y1
Y4 = SIGN(YY4,Y4SGN)
YY5 = BB*SQRT(1.-X5**2/RAD**2)
YY5SGN = X5*CTNU+Y1
Y5 = SIGN(YY5,Y5SGN)
B1 = SQRT((Y4-Y1)**2+(X4-X1)**2)
B2 = SQRT((Y5-Y1)**2+(X5-X1)**2)
1) #2+(X1-X21)**2))
DNL2 = ARCCOS(Y1*(Y1-Y22)/(Y1-Y21))
1) #2+(X1-X22)**2))
MLL = ATAN(B2/Z)
MLL = ATAN(B1/Z)
NULL = NUO+DNU1
NULL = NUO-DNU2

```

165

```

1) #2+(X1-X21)**2))
DNL2 = ARCCOS(Y1*(Y1-Y22)/(Y1-Y21))
1) #2+(X1-X22)**2))
MLL = ATAN(B2/Z)
MLL = ATAN(B1/Z)
NULL = NUO+DNU1
NULL = NUO-DNU2

```

2410  
2420  
2430  
2440  
2450  
2460  
2470  
2480  
2490  
2500  
2510  
2520  
2530  
2540  
2550  
2560  
2570  
2580  
2590  
2600  
2610  
2620  
2630  
2640  
2650  
2660  
2670  
2680  
2690  
2700  
2710  
2720  
2730  
2740  
2750  
2760  
2770  
2780  
2790  
2800  
2810  
2820  
2830  
2840  
2850  
2860  
2870  
2880

```

GC TO 185
CALCULATION OF INTEGRATION LIMITS FOR THE SURFACE PROJECTION
OF THE POINT OF OBSERVATION INSIDE THE BEAM:
REF 3: EQNS 13,14,43-45,71-77
X1 = -(Z*TAN(MUO))*TAN(NUO))/SQRT(1.+TAN(NUO)**2)
Y1 = -(Z*TAN(MUO))/SQRT(1.+TAN(NUO)**2)
IF ((NUO.EQ.0.).OR.(NUO.EQ.PI)) GC TO 175
X6 = (COTAN(NUO))*(X1*COTAN(NUO)-Y1)+SQRT((BB**2*COTAN(NUO)**2)-(BB**
2NLC)**2+BB**2/RAD**2)
Y6 = BB*SQRT(1.-X6**2/RAD**2)
Y6SG = Y1+(X6-X1)*COTAN(NUO)
Y6 = SIGN(Y6,Y6SG)
GC TO 180
175 Y6 = 0
18C B3 = SQRT((Y6-Y1)**2+(X6-X1)**2)
      MUU = ATAN(B3/Z)
      MLL = 0.*PI
      NLL = 2.*PI
      NUL = 0.

```

```

PRATIO=POWER DENSITY RATIO
COMPUTED USING A TWO-POINT GAUSS-LEGENDRE QUADRATURE
NUMERICAL INTEGRATION SCHEME
REF 3: EQN 53
REFS 14&15
CINT=CONSTANT DURING INTEGRATION
ICP)*((MUU-MUL)*(NUU-NUL))/4.)*CTF
ETAMU1 = ((MUU-MUL)*ETA1+MUU*MUL)/2.
ETAMU2 = ((MUU-MUL)*ETA2+MUU*MUL)/2.
XINU1 = ((NUU-NUL)*XI1+NUU*NUL)/2.
XINU2 = ((NUU-NUL)*XI2+NUU*NUL)/2.
FXT1 = COS(ETAMU1)*COS(MUO)+SIN(ETAMU1)*SIN(MUO)*COS(ABS(XINU1-NUO
1))
FXT2 = COS(ETAMU1)*COS(MUO)+SIN(ETAMU1)*SIN(MUO)*CCS(ABS(XINU2-NUO
1))
FXT3 = COS(ETAMU2)*COS(MUO)+SIN(ETAMU2)*SIN(MUO)*CCS(ABS(XINU2-NUO
1))
FXT4 = COS(ETAMU2)*COS(MUO)+SIN(ETAMU2)*SIN(MUO)*CCS(ABS(XINU1-NUO
1))
FRATIO = ABS(CINT*(FXT1+FXT2+FXT3+FXT4))

```

```

PWRDEN(J) = 10.*ALOG10(PRATIO*Z**2)
REF 2: PGS 65-67; FIG 34
CUTPUT INSTRUCTIONS

```



FAR ZONE COMPUTER PROGRAM

10  
20  
30  
40  
50  
60  
70  
80  
90  
100  
110  
120  
130  
140  
150  
160  
170  
180  
190  
200  
210  
220  
230  
240  
250  
260  
270  
280  
290  
300  
310  
320  
330  
340  
350  
360  
370  
380  
390  
400  
410  
420  
430  
440  
450  
460  
470  
480

FAR ZONE SOLUTION OF THE TIME-AVERAGE POWER PROBABILITY  
DISTRIBUTION BELOW THE OCEAN OF A LASER BEAM INCIDENT  
ON THE SURFACE

NCMENCLATURE:

PSI=ANGLE OF INCIDENT BEAM WITH RESPECT TO VERTICAL AXIS  
CHI=ANGLE OF WIND WITH RESPECT TO THE INCIDENT BEAM IN  
THE XY-PLANE  
ALPHA=ANGLE OF MAX WAVE SLOPE WITH RESPECT TO THE INCIDENT  
BEAM IN THE XY-PLANE  
B=MAX SLOPE OF WAVE FACET  
NU=NUO=ANGLE BETWEEN REFRACTED RAY PROJECTED ONTO XY-PLANE  
AND THE Y AXIS  
MU=MUO=ANGLE BETWEEN REFLECTED RAY AND THE Z AXIS  
Z=DEPTH BELOW OCEAN SURFACE (METERS)  
RAD=INCIDENT RAY SPOT RADIUS AT WAVE FACET (MINOR AXIS OF  
ELLIPSE WHEN PSI IS NON-ZERO)  
BB=MAJOR AXIS OF SPOT INCIDENT ON WAVE FACET  
W=WIND VELOCITY (M/SEC)  
WI=RAY INCIDENCE ANGLE  
WR=RAY REFRACTION ANGLE  
LTF=DIFFUSE TRANSMITTANCE FUNCTION  
BS=BACKWARD SCATTERING COEFFICIENT  
AC=ABSORPTION COEFFICIENT  
T=FRESNEL'S TRANSMITTANCE FUNCTION  
AN=INDEX OF REFRACTION  
PSLOPE=SLOPE PROBABILITY FUNCTION  
DAREA=AREA INCREMENT  
JACOB=JACOBIAN  
PWRDEN=POWER DENSITY (DECIBELS)

INTEGER VALID  
REAL NUO, JMUO, JACOB, MLO, NUORUN  
COMMON MUO, NUO, PSI, AN, PSIRUN, NUORUN, PI, Z, RAD, BB, JK  
DIMENSION W(3), CHI(3), NCHI(3), RG(4), JMUC(90), PWRDEN(90), PSIN  
1(1C)

INFUT PARAMETERS:  
DATA W, CHI, NCHI/ 14., 10., 5., 0., 1., 5708, 3., 1415., 0., 90., 180/  
DATA PSIN/ 0., 10., 20., 30., 40., 50., 60., 70., 80., 84./  
Z = 50.  
RAD = .2  
PI = 3.141592654  
AN = 1.33  
NUORUN = 0.

CCCCCCCCCCCCCCCCCCCCCCCCCCCCCCCCCCCC

C



```

570 JMLO(J) = FLOAT(J)
580 MLC = JMUO(J)/57.2958
590 JK = J
1000 J = J-6
1010 ALPHA,B,WI,WR ARE COMPUTED IN SUBROUTINE ANGLES:
1020 REFS 2,3&4
1030 CALL ANGLES (ALPHA,B,WI,WR)
1040 T=FRESNEL'S TRANSMITTANCE
1050 REFS 9&10
1060 TPER = (2.*COS(WI)*SIN(WR)/SIN(WI+WR))**2
1080 TPAR = (2.*COS(WI)*SIN(WR)/SIN(WI+WR)*COS(WI-WR))**2
1090 T = (TPAR+TPER)/2.
1100
1110 JACOBIAN COMPUTED IN SUBROUTINE JACO
1120 REF 3: EQNS 48-52
1130 CALL JACO (ALPHA,B,JACOB)
1140
1150 AREA INCREMENT (DAREA) COMPUTED IN SUBROUTINE AREA
1160 REF 3: EQNS 13,14,21-24,38,39,79,80
1170 CALL AREA (DAREA)
1180
1190 FSLCPE=SLOPE PROBABILITY FUNCTION
1200 REF 5: EQNS 5-9,12-18
1210 SIGC = SQRT(.003+1.92E-03*W(I))
1220 SIGU = SQRT(3.16E-03*W(I))
1230 C21 = .01-.0086*W(I)
1240 C40 = .04-.033*W(I)
1250 C42 = .4
1260 C44 = .12
1270 C23 = .23
1280 AP = ALPHA-CHI(L)
1290 ZXP = TAN(B)*SIN(AP)
1300 ZYP = TAN(B)*COS(AP)
1310 XI = ZXP/SIGC
1320 ETA = ZYP/SIGU
1330 FACT1 = (1./(2.*PI*SIGC*SIGU))*EXP(-.5*(XI**2+ETA**2))
1340 FACT2 = 1.-.5*C21*(XI**2-1.)*ETA-(1./6.)*C03*(ETA**3-3.*ETA)
1350 FACT3 = (1./24.)*C40*(XI**4-6.*XI**2+3.)*+.25*C22*(XI**2-1.)*(ETA**
1360 -1.)
1370 FACT4 = (1./24.)*C04*(ETA**4-6.*ETA**2+3.)
1380 FSLCPE = FACT1*(FACT2+FACT3+FACT4)
1390
1400 VALIDITY CHECK (VALID=1; INVALID=0) ON SLCPE PROBABILITY
1410 AXI = ABS(XI)
1420 AETA = ABS(ETA)
1430 VALID = 1
1440

```



COMMON COMPUTER SUBROUTINES

```

10
20
30
40
50
60
70
80
90
100
110
120
130
140
150
160
170
180
190
200
210
220
230
240
250
260
270
280
290
300
310
320
330
340
350
360
370
380
390
400
410
420
430
440
450
460
470
480

SUBROUTINE ANGLES ( ALPHA,B,WI,WR)
SUBROUTINE ANGLES SOLVES FOR ALPHA,B,WI&WR GIVEN PSI,NUO,MUO&AN
EXTERNAL FINDAB,FINDB
REAL NUC,MUO,NUORUN
COMMON MUO,NUO,PSI,AN,PSIRUN,NUORUN,PI,Z,RAC,EB,JK
DIMENSION Q(2),Y(1)
IF (PSIRUN.EQ.0.) GO TO 230
IF (NUORUN.EQ.0.) GO TO 215

SOLUTION FOR PSI&NUO NON-ZERO:
ALPHA & B FOR A GIVEN MUO & NUO ARE OBTAINED BY SOLVING
SIMULTANEOUS NON-LINEAR EQNS 82&83 OF REF 3 USING IBM SOURCE
LIB SUBROUTINE (NLNSYS)

FIRST ESTABLISH INITIAL GUESS FOR NLNSYS
IF ((JK.EQ.1).OR.((JK.EQ.15).AND.(PSIRUN.GT.30.))) GO TO 205
Q(1) = ALPHA
Q(2) = B
GC TO 210
205 Q(1) = .1
210 Q(2) = .1
CALL NLNSYS (2,10,4,ISING,1,FINDAB,Q)
B = Q(2)
WI = ARCCOS(COS(PSI)*COS(B)-SIN(PSI)*COS(ALPHA)*SIN(B))
WR = ARCCOS((1./AN)*SQRT(COS(WI)**2+AN**2-1.))
GC TO 235

SOLUTION FOR PSI NON-ZERO & NUO=0.0:
ALPHA = 0.
B SOLVED FROM NON-LINEAR EQN 82 OF REF 3 USING IBM SOURCE LIB
SUBROUTINE (NLNSYS); FIRST ESTABLISH INITIAL B GUESS
IF ((JK.EQ.1).OR.((JK.EQ.15).AND.(PSIRUN.GT.30.))) GO TO 220
Y(1) = B
GC TO 225
220 Y(1) = .1
225 CALL NLNSYS (1,10,4,ISING,1,FINDB,Y)
B = Y(1)
WI = ARCCOS(COS(PSI)*COS(B)-SIN(PSI)*SIN(B))
WR = ARCCOS((1./AN)*SQRT(COS(WI)**2+AN**2-1.))
GC TO 235

SOLUTION FOR PSI=0.0:
ALPHA = NUO
B = ATAN((AN*SIN(MUO))/(AN*COS(MUO)-1.))
WI = B

```

C 235  
MR = ARSIN((1./AN)\*SIN(B))  
RETURN  
END

490  
500  
510  
520





```

10 SLROUTINE JACO (ALPHA,B,JACOB)
20
30 SLROUTINE JACO COMPUTES THE JACOBIAN FOR NORMAL & OBLIQUE
40 INCIDENCE.
50
60 REAL JACOB,MUO,NUO,NUORUN
70 CCMCN,MUO,NUO,PSI,AN,PSIRUN,NUORUN,PI,Z,RAC,BB,JK
80 IF (PSIRUN.EQ.0.) GO TO 505
90
100 JACCBIAN FOR OBLIQUE INCIDENCE:
110 AKK = SQRT((SIN(PSI)*COS(ALPHA)*SIN(B)-COS(PSI)*COS(B))**2+AN**2-1
120 )
130 SK = (SIN(PSI)*COS(ALPHA)*SIN(B)-COS(PSI)*COS(B))/AKK
140 LKCA = ((SIN(PSI)*SIN(ALPHA)*SIN(B)-COS(PSI)*COS(B))/AKK
150 +SIN(ALPHA)*SIN(B))/AKK
160 DKCB = ((SIN(PSI)*COS(ALPHA)*SIN(B)-COS(PSI)*COS(B))*SIN(PSI)*CO
170 S(ALPHA)+COS(B)+COS(PSI)*SIN(B))/AKK+(SIN(PSI)*COS(ALPHA)*COS(B)
180 +COS(PSI)*SIN(B))
190 D = ((SK*SIN(ALPHA)*SIN(B))**2+(SK*COS(ALPHA)*SIN(B)-SIN(PSI))**2)
200 /SQRT(AN**2-(COS(PSI)+SK*COS(B))**2)
210 JACOB = ABS((1./D)*(COS(B)*SIN(ALPHA)*SIN(PSI)*DKCA)*(OKDB*SIN(B)
220 +SK*COS(B))+DKDB*COS(B)-SK*SIN(B))*((SK*SIN(B))**2-(SIN(PSI)*SIN(
230 B))*DKDA*SIN(ALPHA)+SK*COS(ALPHA)))
240 GC TO 510
250
260 JACOBIAN FOR NORMAL INCIDENCE:
270 AK = -CCS(B)+SQRT(COS(B)**2+AN**2-1.)
280 DKCB = SIN(B)*((1.-(COS(B)/SQRT(COS(B)**2+AN**2-1.)))
290 JACOB = ABS((1./SQRT(AN**2-(1.+AK*COS(B))**2))*DKCB*COS(B)-AK*SIN
300 I(B)))
310
320 RETURN
330 ENC

```

```

10 SLROUTINE AREA (DAREA)
20 SLROUTINE AREA COMPUTES THE AREA INCREMENT (DAREA) FOR
30 NORMAL & OBLIQUE INCIDENCE.
40
50 REAL MLO,NUO,NUORUN
60 COMMON MUO,NUO,PSI,AN,PSIRUN,NUORUN,PI,Z,RAC,BB,JK
80 CALL ERRSET (251,500,-1,1)
90 IF (PSIRUN.EQ.0.) GO TO 625
100
110 CAREA FOR OBLIQUE INCIDENCE:
120 X1 = -(Z*TAN(MUO)*TAN(NUO))/SQRT(1.+TAN(NUO)**2)
130 Y1 = -(Z*TAN(MUO))/SQRT(1.+TAN(NUO)**2)
140 INTERMEDIATE EQNS: ABX,AYS,BXAY
150 ABX = (RAD**2)*(BB**2)*X1
160 AYS = (RAD**2)*Y1*SQRT((BB**2)-(RAD**2)-(RAD**2)+(RAD**2))*
170 1Y1**2)
180 BXAY = (BB**2)*(X1**2)+(RAD**2)*(Y1**2)
190 X21 = (ABX-AYS)/BXAY
200 X22 = (ABX+AYS)/BXAY
210 IF (X1.LT.RAD) GO TO 605
220 Y21 = BB*SQRT(1.-X21**2/RAD**2)
230 Y22 = BB*SQRT(1.-X22**2/RAD**2)
240 GC TO 610
250 Y21 = -BB*SQRT(1.-X21**2/RAD**2)
260 Y22 = -BB*SQRT(1.-X22**2/RAD**2)
270 IF (NUO.NE.0.) GO TO 615
280 X4 = 0.
290 X5 = 0.
300 Y4 = -BB
310 Y5 = BB
320 GC TO 620
330 CTNU = CO TAN(NUO)
340 CA = CTNU*(X1*CTNU-Y1)
350 CB = SQRT(BB**2*CTNU**2-(BB**2/RAD**2)*(Y1**2-BB**2+X1*CTNU*(X1*CT
360 1NU-2.*Y1)))
370 CC = CTNU**2+BB**2/RAD**2
380 X4 = (CA-(SIN(NUO))/ABS(SIN(NUO)))*CB)/CC
390 X5 = (CA+(SIN(NUO))/ABS(SIN(NUO)))*CB)/CC
400 Y4 = BB*SQRT(1.-X4**2/RAD**2)
410 Y4SG = (X4-X1)*CTNU+Y1
420 Y4 = SIGN(Y4,Y4SG)
430 Y5 = BB*SQRT(1.-X5**2/RAD**2)
440 Y5SG = (X5-X1)*CTNU+Y1
450 Y5 = SIGN(Y5,Y5SG)
460 C1 = SQRT((Y5-Y1)**2+(X5-X1)**2)/Z
470 C2 = SQRT((Y4-Y1)**2+(X4-X1)**2)/Z
480 C3 = (Y1*(Y1-Y21)+X1*(X1-X21))/SQRT((X1**2+Y1**2)*((Y1-Y21)**2+(X1

```

```

490 1-X21)**2))
500 C4 = (Y1*(Y1-Y22)+X1*(X1-X22))/SQRT((X1**2+Y1**2)*((Y1-Y21)**2+(X1
510 1-X21)**2))
520 IF (C3.GT.1.0) C3 = 1.0
530 IF (C4.GT.1.0) C4 = 1.0
540 LAREA = ((PI/4.)*(ATAN(C1)-ATAN(C2)))*(ARCCOS(C3)+ARCCOS(C4))
550 GC TO 640
560
570
580
590
600
610
620
630
640
650
660
670
680
690
700
710
720
730
740
750
760
770
780
790
800
810
820
830
840
850
860
870
880
890
900
910
920
930

C
625 LAREA FCR NORMAL INCIDENCE:
X1 = 0.
Y1 = -Z*TAN(MUO)
X22 = -(RAD*Y1*SQRT(Y1**2-RAD**2))/Y1**2
X21 = -X21
Y22 = -RAD*SQRT(1.-X21**2/RAD**2)
Y21 = -RAD*SQRT(1.-X22**2/RAD**2)
IF (MUO.NE.0.) GO TO 630
X4 = 0.
X5 = 0.
Y4 = -RAD
Y5 = RAD
GC TO 635

630 CTNU = COTAN(MUO)
CNA = -Y1*CTNU
CNB = SQRT(ABS(RAD**2*CTNU**2-Y1**2+RAD**2))
CNC = CTNU**2+1.
X4 = (CNA-(SIN(MUO)/ABS(SIN(MUO))))*CNB)/CNC
X5 = (CNA+(SIN(MUO)/ABS(SIN(MUO))))*CNB)/CNC
Y4 = BB*SQRT(1.-X4**2/RAD**2)
Y4SGN = X4*CTNU+Y1
Y4 = SIGN(Y4,Y4SGN)
Y5 = BB*SQRT(1.-X5**2/RAD**2)
Y5SGN = X5*CTNU+Y1
Y5 = SIGN(Y5,Y5SGN)
C1 = SQRT((Y5-Y1)**2+(X5-X1)**2)/Z
C2 = SQRT((Y4-Y1)**2+(X4-X1)**2)/Z
C3 = (Y1*(Y1-Y21)+X1*(X1-X21))/SQRT((X1**2+Y1**2)*((Y1-Y21)**2+(X1
1-X21)**2))
C4 = (Y1*(Y1-Y22)+X1*(X1-X22))/SQRT((X1**2+Y1**2)*((Y1-Y21)**2+(X1
1-X21)**2))
IF (C3.GT.1.0) C3 = 1.0
IF (C4.GT.1.0) C4 = 1.0
LAREA = ((PI/4.)*(ATAN(C1)-ATAN(C2)))*(ARCCOS(C3)+ARCCOS(C4))
C
640 RETURN
END

```



```

C          IF PARTIAL IS TOO SMALL, INCREASE TALLY.
          IF (ABS(PART(I,TEMP)).EQ.0) GO TO 9
          IF (ABS(F/PART(I,TEMP)).GT.1.0E20) TALLY=TALLY+1
          GO TO 10
          TALLY=TALLY+1
          9 CCNTINUE
          10 IF (TALLY.LE.(N-K)) GO TO 15
          FACTOR=FACTOR*10.0
          IF SURFACE IS TOO FLAT, THE SINGULARITY INDICATOR IS SET TO C
          ZERO AND RETURN IS EXECUTED.
          IF (FACTOR.GT..5) GO TO 65
          15 IF (K.LT.N) GO TO 20
          IF LAST PARTIAL IS ZERO, A SINGULARITY IS INDICATED AND A
          RETURN EXECUTED.
          IF (ABS(PART(I,TEMP)).EQ.0.) GO TO 65
          CCE(K,N+1)=0
          KMAX=ITEMP
          20 KMAX=PONTER(K,K)
          DERM=ABS(PART(KMAX))
          KPLUS=K+1
          GET INDEX FOR LARGEST PARTIAL IN K*TH EQUATION.
          DC 30 I=KPLUS,N
          JSUB=PONTER(K,I)
          TEST=ABS(PART(JSUB))
          IF (TEST.LT.DERM) GO TO 25
          DERM=TEST
          DEFINE PIVOT TO SWIVEL ABOUT THE VARIABLE WITH MAXIMUM PARTIAL
          WHEN WE GET TO THE NEXT EQUATION.
          PCNTER(KPLUS,I)=KMAX
          IF THIS PARTIAL IS BIGGER, WE HAVE A NEW MAXIMUM.
          KMAX=JSUB
          25 PCNTER(KPLUS,I)=JSUB
          30 CCNTINUE
          IF THAT PARTIAL IS 0, INDICATE A SINGULARITY AND RETURN.
          IF (ABS(PART(KMAX)).EQ.0) GO TO 65
          ISUB(K)=KMAX
          DC 35 J=KPLUS,N
          JSUB=PONTER(KPLUS,J)
          US=J
          SAVE THESE CONSTANTS FOR FUTURE USE.
          CCE(K,J SUB)=-PART(JSUB)/PART(KMAX)
          GET PART OF EXPRESSION FOR THE NEW X(KMAX) VALUE
          CCE(K,N+1)=COE(K,N+1)+PART(JSUB)*X(JSUB)
          35 CCE(K,N+1)=(COE(K,N+1)-F)/PART(KMAX)+X(KMAX)
          40 CCE(K,N IS 1, WE HAVE OUR SOLUTION IN THE NEXT STEP WITHOUT ANY
          C

```

```

NLNS1880
NLNS1890
NLNS1891
NLNS1892
NLNS1893
NLNS1910
NLNS1920
NLNS1930
NLNS1940
NLNS1950
NLNS1960
NLNS1970
NLNS1980
NLNS1990
NLNS2000
NLNS2010
NLNS2020
NLNS2030
NLNS2040
NLNS2050
NLNS2060
NLNS2070
NLNS2080
NLNS2090
NLNS2100
NLNS2110
NLNS2120
NLNS2130
NLNS2140
NLNS2150
NLNS2160
NLNS2170
NLNS2180
NLNS2190
NLNS2200
NLNS2210
NLNS2220
NLNS2230
NLNS2240
NLNS2250
NLNS2260
NLNS2270
NLNS2280
NLNS2290
NLNS2300
NLNS2310
NLNS2320
NLNS2330

```

```

C      BACK-SUBSTITUTING.
C      X(KMAX)=COE(N,N+1)
C      FOR N GREATER THAN 1, WE PERFORM A FINAL BACK-SUBSTITUTION TO
C      GET OUR NEW X-VECTOR.
C      IF (N.GT.1) CALL BAKSUB(N,N,X)
C      IF (M.EQ.1) GO TO 50
C      DC 43 I=1,N
C      IF TEST FOR CONVERGENCE.
C      IF (ABS((TEMP(I)-X(I))/X(I)).GT.RELCON) GO TO 45
C      CCNTINUE
C      CCNVRG=CCNVRG+1
C      IF IT CONVERGES, RETURN WITH LAST VECTOR.
C      IF (CONVRG.GE.3) GO TO 60
C      CC TO 50
C      CCNVRG=1
C      SAVE CURRENT X-VECTOR FOR TESTING WITH NEXT X-VECTOR.
C      DC 55 I=1,N
C      TEMP(I)=X(I)
C      IF M IS THE ITERATION LIMIT, RETURN.
C      CC TO 70
C      MAXIT=M
C      CC TO 70
C      ISING=1
C      RETURN
C      70  ENCL

```

```

NS2340
NLNS2350
NLNS2360
NLNS2370
NLNS2380
NLNS2390
NLNS2400
NLNS2410
NLNS2420
NLNS2430
NLNS2440
NLNS2450
NLNS2460
NLNS2470
NLNS2480
NLNS2490
NLNS2500
NLNS2510
NLNS2520
NLNS2530
NLNS2540
NLNS2550
NLNS2560
NLNS2570
NLNS2580

```



#### LIST OF REFERENCES

1. Karp, S., " Optical Communications Between Underwater and Above Surface (Satellite) Terminals", IEEE Transactions on Communications, v. 24, p. 66-81, January 1976.
2. Antenna Laboratory, The Ohio State University Research Foundation, Report 1675-3, The Power Probability Distribution Below the Ocean Surface of Diffuse and Collimated Incident Optical Energy, by J. P. Swennen, 21 December 1964.
3. Antenna Laboratory, The Ohio State University Research Foundation, Report 2170-1, Power Density Probability Distribution Below the Ocean Surface of a Beam of Collimated Optical Radiation Obliquely Incident on the Surface, by J. P. Swennen, 31 March 1966.
4. Swennen, J. P., " Time-Average Power-Density Distribution Below the Ocean Surface of a Beam of Collimated Optical Radiation Incident on the Surface", Journal of the Optical Society of America, v. 50, p. 224-229, February 1966.
5. Cox, C. S. and Munk, W. H., " Measurement of the Roughness of the Sea Surface from Photographs of the Sun's Glitter", Journal of the Optical Society of America, v. 44, p. 838-850, November 1954.
6. Groen, P., The Waters of the Sea, p. 122-185, Van Nostrand Reinhold, 1969.
7. New York University Department of Meteorology and

Oceanography Geophysical Sciences Laboratory Report 63-15, The Interpretation of Wave Spectra in Terms of the Wind Profile Instead of the Wind Measured at a Constant Height, by W. J. Pierson, Jr., 1963.

8. Hill, M. N., The Sea-Ideas and Observations on Progress in the Study of the Seas, p. 567-589, 664-699, Wiley, 1962.
9. Born, M. and Wolf, E., Principles of Optics, p. 36-51, Pergamon Press, 1975.
10. Fowles, G. R., Introduction to Modern Optics, p. 33-60, Holt, Rinehart and Winston, 1968.
11. Duntley, S. Q., "The Optical Properties of Diffusing Materials", Journal of the Optical Society of America, v. 32, p. 61-70, February 1942.
12. Tyler, J. E., "Scattering Properties of Distilled and Natural Waters", Limnology and Oceanography, v. 6, p. 451, October 1961.
13. Duntley, S. Q., "Light in the Sea", Journal of the Optical Society of America, v. 53, p. 214-233, February 1963.
14. Carnahan, B., Luther, H. A. and Wilkes, J. O., Applied Numerical Methods, p. 101-116, Wiley, 1969.
15. Gerald, C. F., Applied Numerical Analysis, p. 59-72, Addison-Wesley, 1973.
16. Preisendorfer, R. W., Hydrologic Optics, v. 1-6, U. S. Department of Commerce (NOAA), 1976.
17. Prettyman, C. E. and Cermak, M. D., "The Variation of the Rough Ocean Surface and its Effects on an Incident Laser Beam", IEEE Transactions on Geoscience Electronics, v. 7, p. 235-243, October 1969.

18. Bucher, E. A., " Propagation Models for Optical Communication Through Fog and Clouds", Proceedings of the National Electronics Conference, v. 29, p. 180-185, 1974.

INITIAL DISTRIBUTION LIST

	No. Copies
1. Defense Documentation Center Cameron Station Alexandria, Virginia 22314	2
2. Library, Code 0142 Naval Postgraduate School Monterey, California 93940	2
3. Department Chairman, Code 67 Department of Aeronautics Naval Postgraduate School Monterey, California 93940	1
4. Professor D. J. Collins, Code 67Co Department of Aeronautics Naval Postgraduate School Monterey, California 93940	1
5. Naval Ocean Systems Center, Code 725 Attn: LT Giannaris, USN 271 Catalina Blvd. San Diego, California 92152	1
6. LT Michael J. Milchanowski, USN Air Force Weapons Laboratory Kirtland AFB New Mexico 87115	1